Geomorphology 380 (2021) 107629

Contents lists available at ScienceDirect

Geomorphology

journal homepage: www.elsevier.com/locate/geomorph

Fold architecture predisposing deep-seated gravitational slope deformations within a flysch sequence in the Northern Apennines (Italy)

C. Esposito [a], E. Di Luzio [b,*], M. Baleani [c], F. Troiani [a], M. Della Seta [a], F. Bozzano [a], P. Mazzanti [a,c]

[a] "Sapienza" University of Rome, Earth Science Department, Piazzale Aldo Moro, 5, 00185 Rome, Italy
[b] CNR-IGAG, National Research Council - Institute of Environmental Geology and Geoengineering, Montelibretti, Via Salaria Km 29.3, 00165, Monterotondo St., Rome, Italy
[c] NHAZCA s.r.l., Spin-off "Sapienza" University of Rome, Via Vittorio Bachelet, 12, 00185 Rome, Italy

ARTICLE INFO

Article history:
Received 16 May 2020
Received in revised form 8 December 2020
Accepted 17 January 2021
Available online 29 January 2021

Keywords:
Slope deformation
Mass movement
Fold structure
River dynamics
Northern Apennines

ABSTRACT

This research illustrates the case of a deep-seated gravitational slope deformation (DSGSD) affecting a folded structure that developed during Miocene tectonics in the Northern Apennines of Italy, deforming a heterogeneous turbiditic sequence characterised by pelitic-marly and arenaceous intervals. The investigated area includes the headwater portion of the Bidente River basin that has experienced intensive valley incision during the late Quaternary and the sizeable Poggio Baldi landslide with failure episodes in 1914 and 2010.

The aim of this work was to unravel the local morphostructural setting determined by the interplay between the active DSGSD, inherited fold geometry, and fluvial dynamics. Dip data collection and structural analysis were used to reconstruct the fold geometry. A complex type of fault-propagation fold was outlined, with later breakthrough thrusts causing the backlimb rotation. Gravity-driven geomorphological features were inventoried and displayed on two geological cross-sections together with Geological Strength Index measurements, while their distribution was analysed to conceive a conceptual model for the development of the DSGSD. Fold setting and lithological anisotropies were considered as the predisposing factors of the gravitational slope deformation, whereas the multi-step entrenchment of the Bidente River valley, testified by the presence of the remnants of at least three generations of fluvial erosional terraces, was considered as the main cause of its initiation.

Finally, the reconstruction of the original slope topography in the Poggio Baldi area and the results of structural analysis performed in the landslide detachment zone through remote sensing techniques allowed for the estimation of the size of the wedge-shaped rock block which detached in 1914, an event that occurred in the wider frame of the DSGSD.

1. Introduction

Deep-seated gravitational slope deformations (DSGSDs) consist of large-scale, short-displacement mass movements that can arise and develop into hill slopes and mountain ridges (e.g. Ter-Stepanian, 1966; Zischinsky, 1966; Němčok, 1972; Radbruch-Hall, 1978; Hutchinson, 1988; Dramis and Sorriso-Valvo, 1994). Many authors have demonstrated, from a wide variety of geodynamic and morphoclimatic settings, a specific connection between the development of DSGSDs, as well as large rock slope failures, and inherited structural features (Agliardi et al., 2001, 2009; Kellog, 2001; Di Luzio et al., 2004a, 2004b; Ambrosi and Crosta, 2006; Scarascia-Mugnozza et al., 2006; Esposito et al., 2007, 2013, 2014; Brideau et al., 2009; Bianchi Fasani et al., 2011, 2014; Massironi et al., 2011; Pedrazzini et al., 2011; Saintot et al., 2011; Humair et al., 2013; Soldati, 2013; Coquin et al., 2016; Pánek et al., 2017; Penna et al., 2017; Di Naccio et al., 2019).

Among geological scenarios, the association of folding and gravitational movements including failure events was discussed by Badger (2002), Humair et al. (2013), Stead and Wolter (2015), and Alfaro et al. (2019), among others. Folding of sedimentary rock sequences, in particular, can generate various effects on rock slope stability depending on fold geometry and its orientation with respect to the slope surface. Simple translational failures or toppling can be associated with different limbs of horizontal folds, whereas complex translational or rotational failures are frequently observed in steeply plunging folds (Stead and Wolter, 2015). Fold-related discontinuity sets can concentrate in weakness zones, as in the hinge area, and this can locally decrease the rock mass strength; the same effect can be enhanced by the combination of several tectonic episodes. Finally, rock masses can behave anisotropically, where lithological contrasts are present along folded bedding planes. Therefore, the knowledge of fold geometry, the structural

* Corresponding author.
E-mail addresses: carlo.esposito@uniroma1.it (C. Esposito), emiliano.diluzio@igag.cnr.it (E. Di Luzio), marco.baleani@nhazca.com (M. Baleani), francesco.troiani@uniroma1.it (F. Troiani), marta.dellaseta@uniroma1.it (M. Della Seta), francesca.bozzano@uniroma1.it (F. Bozzano), paolo.mazzanti@uniroma1.it, paolo.mazzanti@nhazca.com (P. Mazzanti).

https://doi.org/10.1016/j.geomorph.2021.107629
0169-555X/

a)

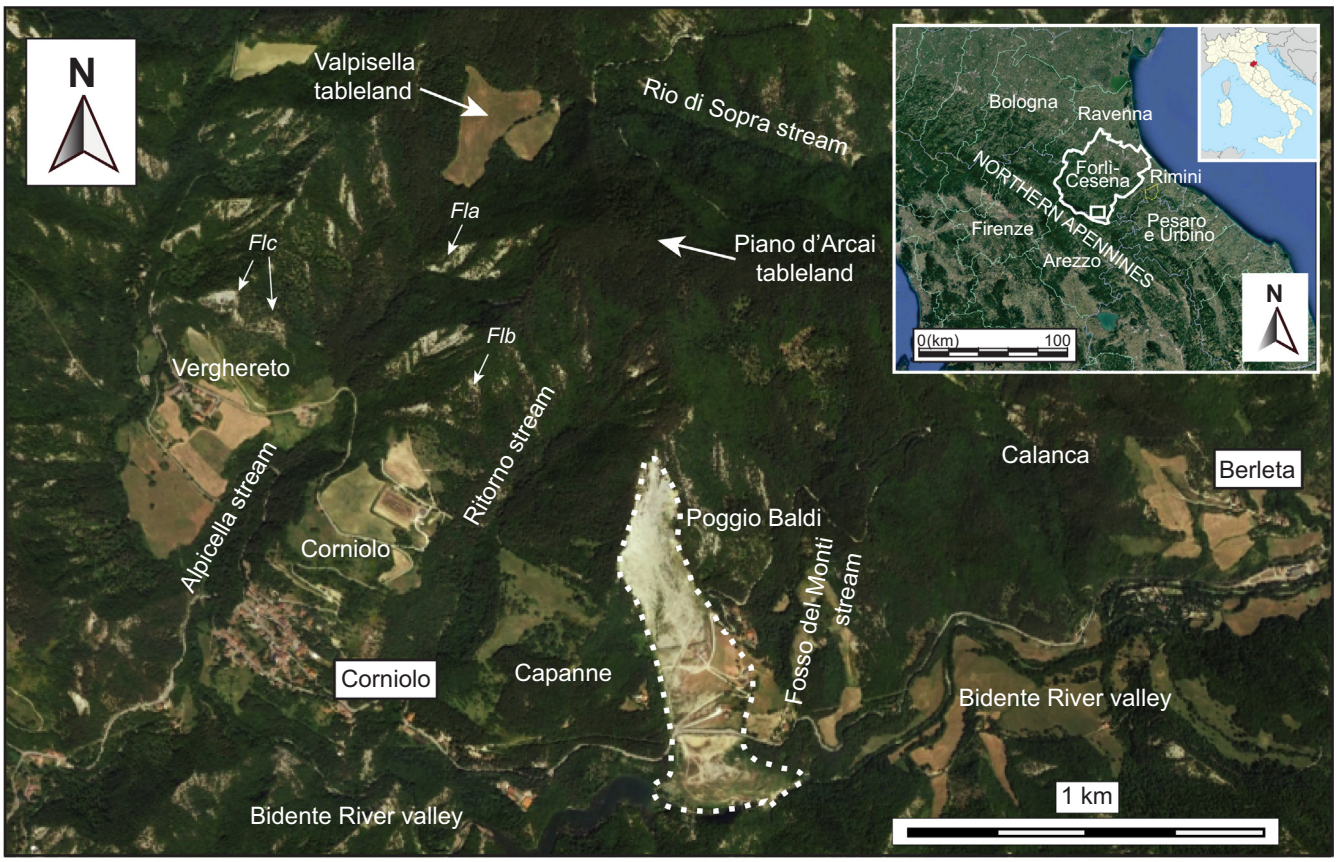

b)

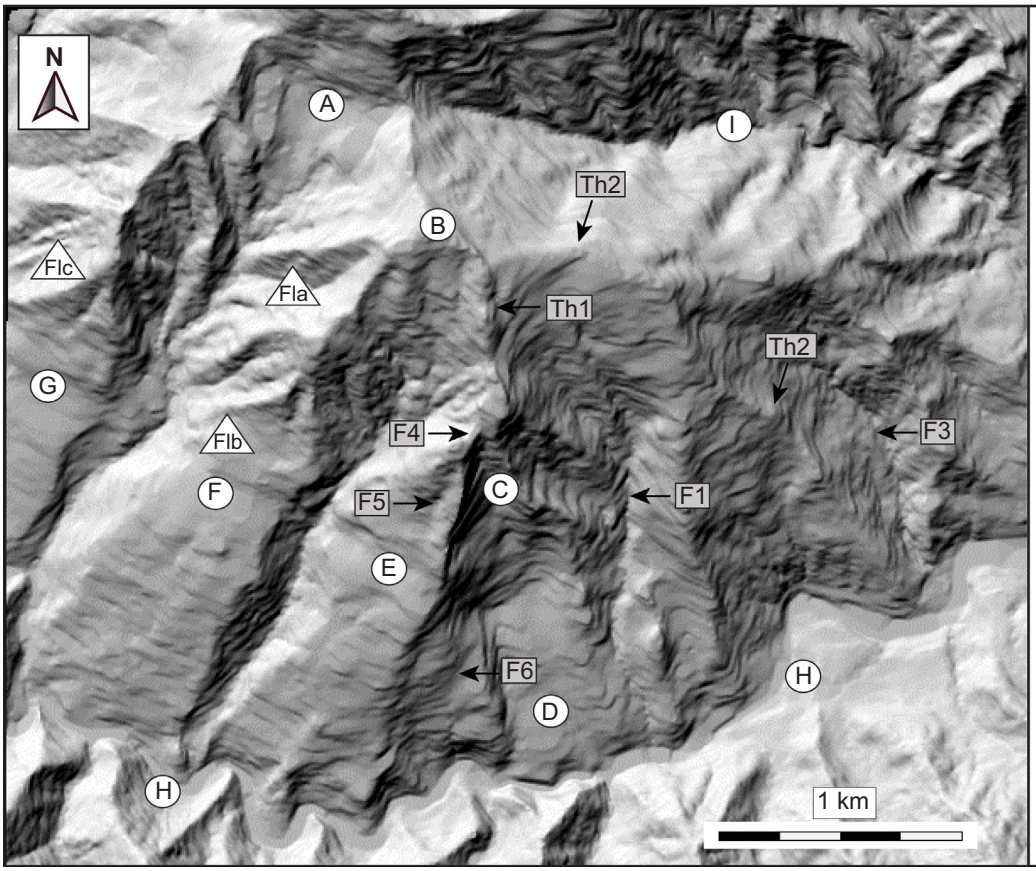

A - Valpisella tableland

B - Piano d'Arcai tableland

C - Poggio Baldi landslide detachment area

D - Poggio Baldi landslide accumulation area

E - Capanne slope

F - Corniolo slope

G - Verghereto slope

H - Bidente River

I - Rio di Sopra stream

F1-F6 - Main faults

Th1-Th2 - Main thrusts

Fla-Flc - Flatiron surfaces

complexity of which can increase as a consequence of multi-stage tectonics, is important for deriving conceptual models of gravity-driven deformations and failure mechanisms.

In this work, to provide further insight into the relationship between DSGSDs and morphostructural features, we present a case study where the kinematic evolution of a fault-propagation fold (e.g. Mitra, 1990; Suppe and Medwedeff, 1990), developed within a turbiditic sequence, has preconditioned the development of a DSGSD process and the onset of a relatively large, still-active rock slope failure zone. Further control of gravitational deformation was exerted by lithological heterogeneities within the flysch sequence (e.g. Pánek et al., 2011, 2017, 2019; Chalupa et al., 2018). The study area is located in the Forlì-Cesena province territory, along the northern valley side of the headwater sector of the Bidente River, in a mountainous area which is part of the axial zone of the Northern Apennines (Fig. 1a, b). Unlike the Alpine domain, where DSGSDs were strongly influenced by Quaternary deglaciation, in the sedimentary cover of the Central-Northern Apennines such process tend to be conditioned by inherited tectonics and slope-to-valley systems morphogenesis (e.g. Di Luzio et al., 2004a, 2004b; Galadini, 2006; Esposito et al., 2007, 2013, 2014; Discenza et al., 2011; Bianchi Fasani et al., 2011, 2014; Moro et al., 2012; Gori et al., 2014; Della Seta et al., 2017).

The main aims of this study were: i) establish the definition of the local geological and morphostructural setting; ii) produce an inventory of diagnostic features revealing an active gravity-driven process; iii) reveal the relationships between the DSGSD, fold structure, and morphoevolution of the Bidente River valley, and iv) reconstruct the rock failure mechanism of the 1914 Poggio Baldi landslide, which represents the first known activation of the sizable failure that involved one flank of the deforming slope (Fig. 2a–d).

Widespread dip data collection and dip domain analysis within the sedimentary multilayer were performed, kinematics of main faults were characterised, and a subsequent inventory of indicative landforms of the DSGSD process was completed. Geomechanical characterisations using the Geological Strength Index (GSI) indicated the presence of weakness zones within the deforming rock slope. For the nearly inaccessible slope sectors, remote sensing methodologies were employed: aerial photogrammetry through an unmanned aerial system (UAS) investigated joint set distribution and geometry of main faults in order to refine the structural and geomechanical model of the slope.

Finally, structural, geomorphological, and geomechanical data were merged together to derive a conceptual model of the multi-step DSGSD process and the original failure mechanism of the Poggio Baldi landslide. The macro-structural frame and lithological heterogeneities in the turbiditic sequence were debated as the main predisposing factors, while the long-term Bidente River valley incision was the principal cause of the lateral unconfinement and the gravitational deformation of the fold structure.

2. Geological framework

The study area is characterised by a turbiditic (flysch) sequence composed of alternating pelites/hemipelagites and arenites with a thickness ranging between 50 and 900 m. This sequence belongs to the early middle Miocene Corniolo member of the Marnoso-Arenacea formation, the latter cropping out extensively in this sector of the Apennine belt (Benini and Farabegoli, 1990; Benini et al., 1991; Farabegoli et al., 1991). Three sedimentary intervals showing a significant prevalence of the pelitic/marly fraction (P) on the arenaceous fraction (A), ($1/3 > A/P > 1/4$), were distinguished in the study area (Figs. 3, 4a, b) in the middle part of the turbiditic sequence (denoted as pml0, pml1, and pml2). Among the lithic arenaceous intervals (Fig. 4c) in the rest of the Corniolo member, the 'Calanca' layer (Ca) is a key-horizon observed near Corniolo village between 550 and 600 m above sea level (a.s.l.) (Fig. 4d) and in the core of the mountain areas (700–750 m a.s.l., Fig. 3). The layer Ca is composed of 3–5 m thick sandstone overlying a basal pelitic horizon, 2–3 m thick. Quaternary continental units, including landslide deposits, talus slope, ancient alluvial fan deposits, and in-channel alluvial deposits (Martelli et al., 2002), complete the geological framework and are mainly found in the downslope areas or along the Bidente River main channel (Fig. 3).

The axial zone of the Northern Apennines is characterised by Quaternary regional uplift and active tectonics that produce low intensity, frequent, recurring earthquakes (e.g. Argnani et al., 2003; De Luca et al., 2009; Martelli et al., 2017). The structural style of mountain ridges was inherited by the Middle Miocene (Tortonian) orogeny, which originated NE-verging thrusts of regional importance and high shortening. In the core of the hanging-wall zones, both high- and low-wavelength folds developed in the sedimentary cover. Minor folds, such as those reconstructed in the Poggio Baldi area, later experienced secondary thrusting with breakthrough geometries and low displacements. Thrusts and folds show significant lateral continuity, which is locally interrupted by transversal faults and shear zones (Farebegoli et al., 1991).

In the Poggio Baldi area, two thrust surfaces (denoted as Th1 and Th2 in Fig. 3) were recognised, which were dissected by NNE-SSW and WNW-ESE-oriented strike-slip faults (F1–F8 in Fig. 3). These last can be associated with the western termination of the Bidente Line, a main strike-slip, left-lateral fault zone which has been active since the Late Miocene and shows neotectonic evidence far from the study area (Benini and Farabegoli, 1990; Farabegoli et al., 1991; Martelli et al., 2002).

3. Geomorphological setting of the Poggio Baldi area

The study area is enclosed in a mountain region characterised by gently-dipping slopes at medium and low elevations (500–700 m a.s.l.). In the higher sectors (700–1000 m), high-dipping morphostructural surfaces prevail with the exception of the Valpisella and Piano d'Arcai tableland extending in the core of the ridge. The local drainage network is characterised by N-S-oriented, deeply incised channels (Valpisella, Ritorno, and Fosso dei Monti streams) flowing southwards into the W-E.-oriented Bidente River main watercourse (Fig. 1a).

Remnants of late Quaternary fluvial terraces, mostly of the erosional type, can be found at different heights above the Bidente River thalweg (Fig. 4e). Terrace remnants are observed on unpaired levels on both sides of the valley, upstream of the Poggio Baldi landslide toe. In general, the erosional (strath) surfaces lack fluvial deposits although, at patches, thin (i.e. <2 m) gravel and sand deposits of fluvial origin can be recognised. The strath terrace remnants are organised in at least three main levels, indicating three abandoned valley floors presently hanging at 140–150, 30–40, and 10–20 m above the thalweg. According to the terrace level classification adopted thus far for the area (Table 1), these hanging valley floors likely correspond to the T1 (or T2?) and T3 terraces of Nesci et al. (2012) coinciding, respectively, to the Qt2, Qt3, and Qt4 + Qt5 + Qt6 terrace levels as re-named in Wegmann and Pazzaglia (2009). The three strath terraces can be correlated among them along the analysed valley; however, difficulties exist in comparing the local terrace sequence with the currently recognised terrace sequence in the middle (eastern) sector of the Bidente River valley by Wegmann and Pazzaglia (2009). Nonetheless, the fluvial terrace morphology, together with their relative heights above the thalweg, allow

Fig. 1. a) Google Earth image of the study area showing the main topographic features and the Poggio Baldi landslide (white, dashed line), upper right inset: geographical frame of the Forlì-Cesena province in the Northern Apennines and location of the study area in the white rectangle; b) hill shade relief map (azimuth 325°; altitude 45°) derived from the "5-m" resolution Digital Elevation Model of the area.

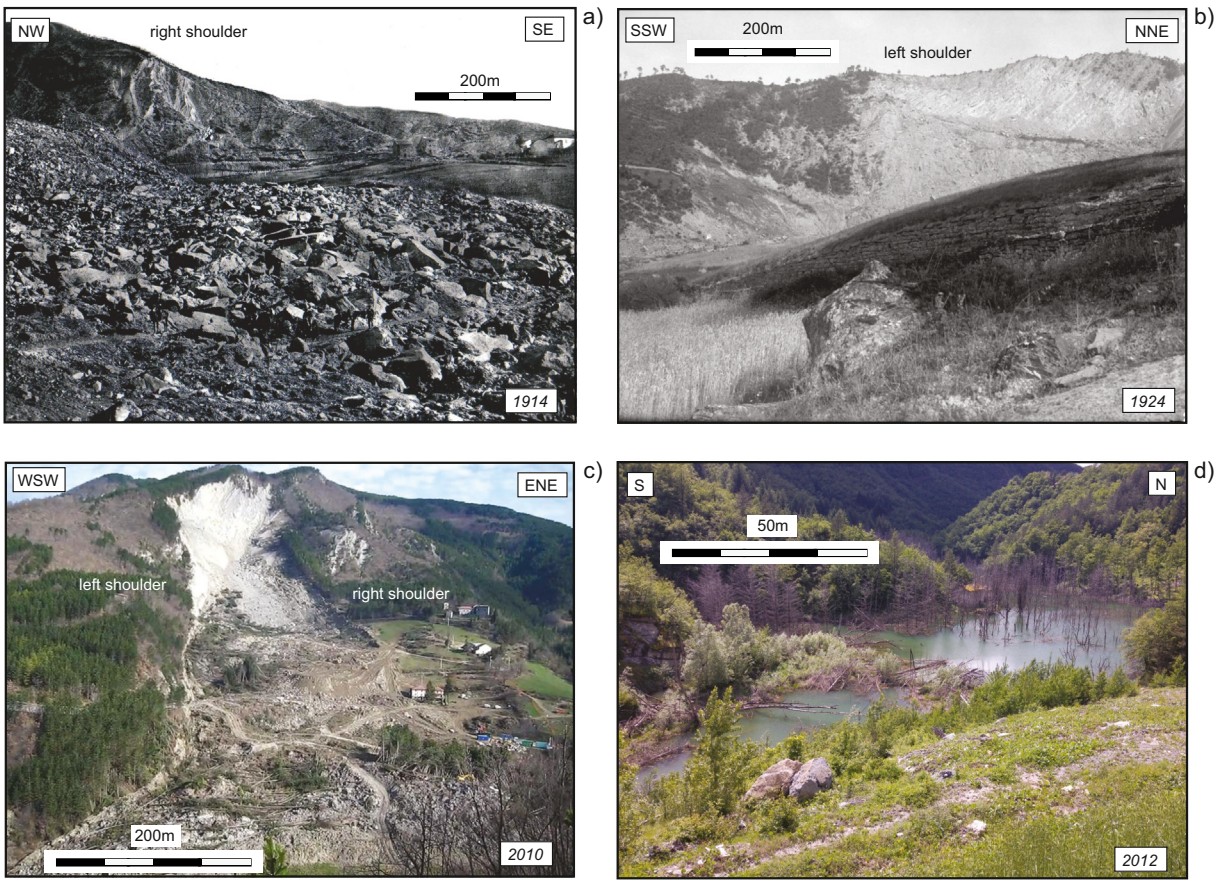

Fig. 2. a) Accumulation area of the Poggio Baldi landslide event on 25th March 1914; b) the Poggio Baldi detachment area in a picture taken in 1924; c) the Poggio Baldi landslide in the week following its reactivation the 18th March 2010; d) the Poggio Baldi barrier lake formed after the 2010 landslide event.

us to infer a reliable relative chronology taking into account the present literature (e.g. Wegmann and Pazzaglia, 2009; Nesci et al., 2012, and references therein). In this context, the local strath terrace chronology is inferred as follows (Table 1): i) middle Pleistocene for the highest level (I); ii) late Pleistocene for the intermediate level (II); and iii) end of late Pleistocene–early Holocene for the lowest and youngest strath terrace level (III).

One of the most prominent geomorphological features of the study area is the Poggio Baldi landslide. The first known reactivation episode (likely the first ever activation) dates back to 25th March 1914, and is thought to have been caused by serious rainfall events as reported by the chronicles of the newspapers of the time. The mountain climate of the Apennines is characterised by harsh, cold winters with abundant snowfall. Frequent rains are concentrated in the spring months, during the same time that the snow melts, as well as in the autumn. Summers are mild and characterised by rare and abundant rain events. Historic photos show a landslide deposit composed of metric sandstone blocks and boulders (Fig. 2a) and a detachment scar with a geometry similar to the one that is currently visible (Fig. 2b, c). Over the course of about one century, the wide and sub-vertical head scarp is thought to have continuously released debris that accumulated on top of the landslide deposit. The overload, combined with an intense and prolonged rainfall and snow melting, triggered the landslide reactivation on 18th March 2010, causing the re-mobilisation of approximately 4×10^6 m^3 of material (Benini et al., 2012; Mazzanti et al., 2017). The landslide mass, with an excessively large movement of debris (950 m long and >350 m wide), obstructed the flow of the Bidente River, causing a rise of 20 m in the water level of the river upstream and forming a barrier lake (Fig. 2c, d). According to Mazzanti et al. (2017), the Poggio Baldi landslide can be classified as complex in terms of style of activity: an original rock slide (1914) was followed by subsequent rock falls that were fed by the resulting high head scarp; produced debris evolved in a composite movement (2010) featuring rotational debris and earth slide (Varnes, 1978; Hungr et al., 2014) and flow slide-like movement (Hutchinson, 1988).

4. Data collection

4.1. Bedding data and main structural features

A collection of dip/dip direction measurements (approximately 250) was completed throughout the study area. Some of these data are shown along two transects in Fig. 5, which pass through the Poggio Baldi and Corniolo slopes along a direction perpendicular to the bedding and thrusts (traces A–A' and B–B′ in Fig. 3). The frequency of field measurements was conditioned by a thick vegetation cover in the northernmost areas. Dip data were assigned to different dip domains whose limits were defined where abrupt changes in dip angles occurred (Δdip value ≥10°). In the western area of transect A–A', dip values ranged between 15° and 25° (Fig. 5a); in correspondence with the Poggio Baldi area, the dip values abruptly increased to 35–45° (Fig. 5b). Moving NE, a short section with bedding inclination that was decreased to 20–35° preceded a wide sector with high-dipping (55–85°) and overturned bedding planes (Fig. 5c), as it could be locally inferred by the presence of ripple marks on the bed roofs (Fig. 5d). Finally, at the eastern termination of the A–A' transect, bedding had again a normal polarity and was gently to moderately inclined (20–35° and 0–20° in Fig. 5a), as also evidenced by an outcrop of the Ca key-horizon (Fig. 5e).

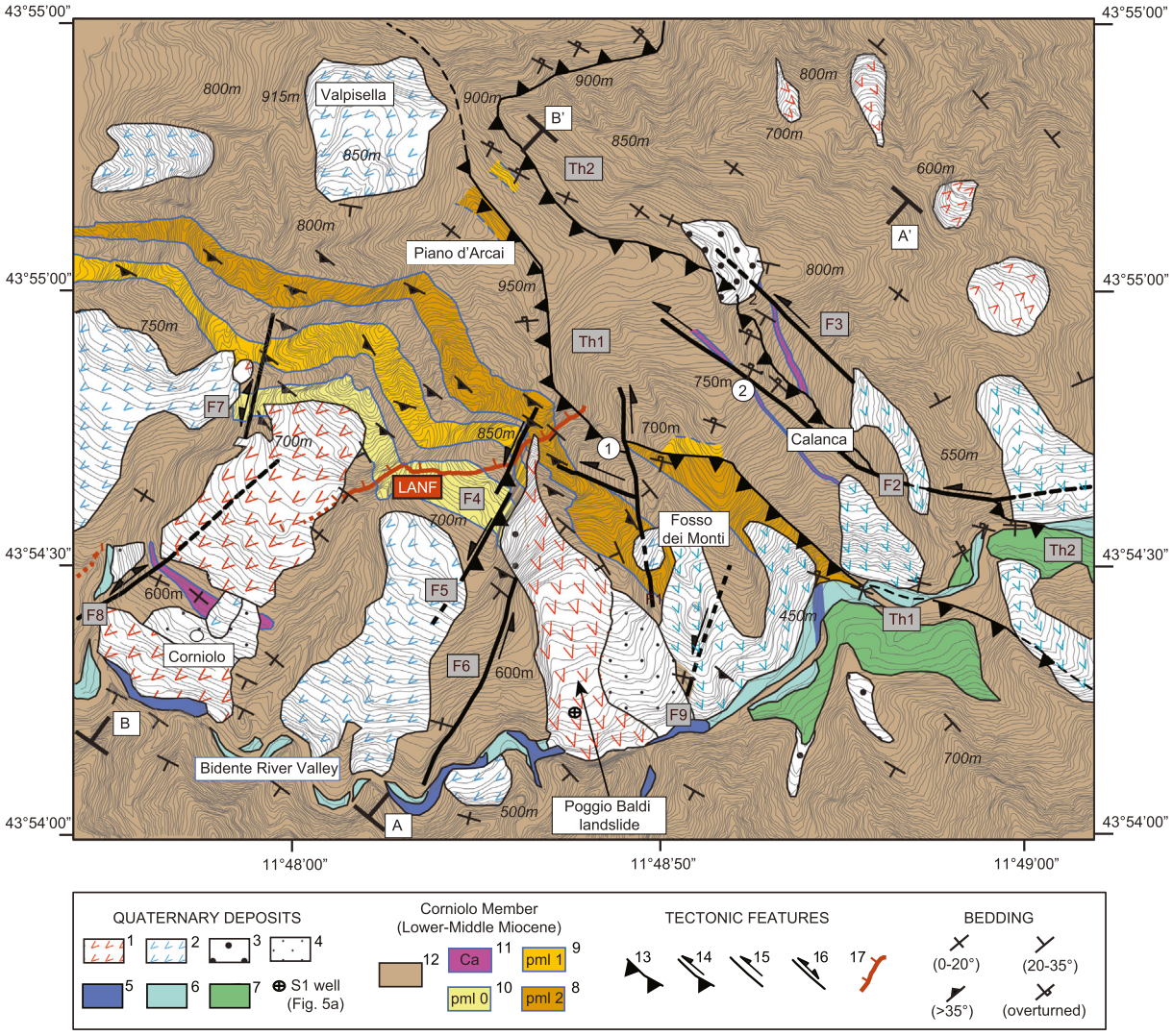

Fig. 3. Geological map of the study area. Continental, post-orogenic deposits are taken from the Geological Map of the Emilia-Romagna region (1:10000 scale). Legend: 1) recent, complex landslide deposits; 2) ancient, complex landslide deposits; 3) debris fan deposits; 4) slope-debris and colluvial deposits; 5) channel gravel and sand deposits; 6) overbank gravel and sand deposits; 7) active and relict alluvial fan deposits); 8), 9), 10) pelitic marly horizons; 11) Calanca (Ca) layer; 12) arenaceous-marly sequence; 13) thrust; 14) transpressive fault; 15) left-lateral, strike-slip fault; 16) strike-slip fault; 17) low-angle normal fault (LANF, Fig. 6a). Labels: F1–F9 = fault codes; 1–2 = structural analysis sites (see plots in Fig. 10a).

The dip data distribution along the Corniolo slope (transect B–B′) was similar, with one central sector (Fig. 5f) where bedding inclination (35–45°) coincided with the slope inclination (Fig. 5g), except for one difference, which was the very low inclined beds (10–20°) located in the westernmost sector and around the Piano d'Arcai tableland (Fig. 5h).

Among the main structural features in the study area, two damaged zones showing thrust-related features were observed along section A–A' (Th1 and Th2 in Fig. 5a). In the Th1 zone, reverse faults cut through the overturned bedding planes of the pml2 horizon with low cut-off angles (Fig. 5c). The Th2 zone, which was characterised by high-density cleavage (Fig. 5e), developed in the eastern sectors at the transition between the overturned beds and the gently west-dipping beds.

Along section A–A', the Poggio Baldi detachment area was characterised by a low-grade tectonic deformation with few but outstanding faults (Fig. 6). A main ENE-WSW-oriented and N-dipping (counter-slope) low-angle normal fault (LANF) was observed at a middle-slope elevation cutting, with a very low displacement and a ramp-flat-ramp geometry, over the entire turbiditic sequence (Fig. 6a). In the same outcrop high-angle, NNE-SSW-oriented faults were observed extending for the entire 100-m high escarpment (Fig. 6b, F4–F6 in Fig. 3), showing a left-lateral, transpressive kinematic also revealed by mesoscale positive flower structures (Fig. 6c).

4.2. Inventory of DSGSD-related features

Several geomorphological features indicative of a gravity-driven process were identified mainly on the Corniolo and Verghereto slopes. Field-observations were integrated by photo-interpretation of aerial and satellite images including: i) coloured four-band orthophoto with a 50-cm pixel size acquired in May–June 2011; ii) aerial photos of the IGMI (Italian Geographic Military Institute), flight 1954–1955; iii) 2010 aerial LIDAR survey (flight altitude of 700 m) of the Emilia-Romagna Region (with a ground pulse density of 4 points/m^2) generating a DTM with a 1 × 1-m resolution.

Different kinds of geomorphic features are homogeneously distributed over an area of about 5 km^2 with a difference in elevation between the Bidente River and the higher parts of the mountain ridge of about 500 m. The features wide and non-random spatial distribution at the mountain scale reveals the presence of a deep-seated gravitational slope deformation. The entire dataset is reported in the map of Fig. 7, together with the strath terraces along the Bidente River valley sides.

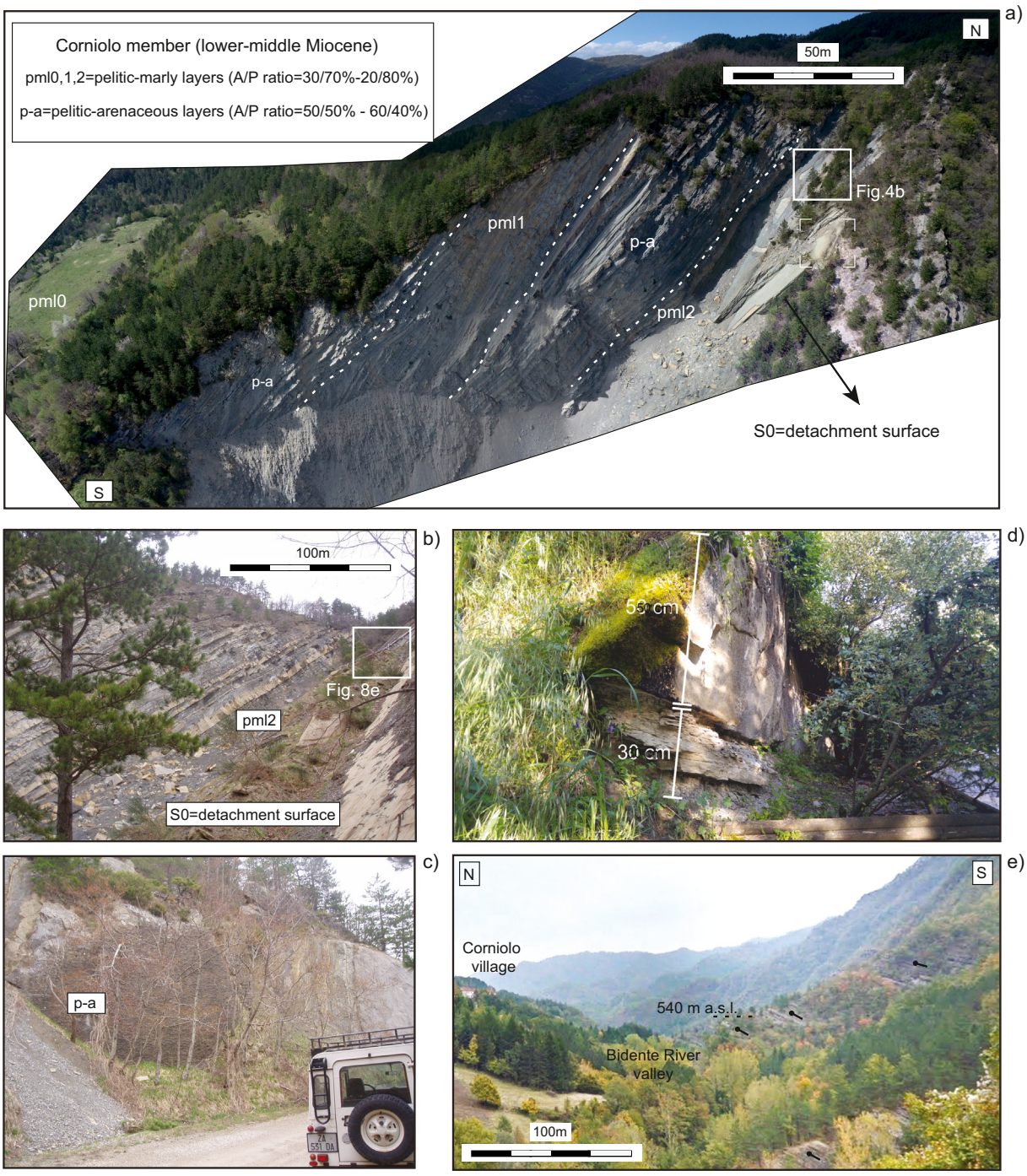

Fig. 4. Geological setting: a) main escarpment on the Poggio Baldi slope evidencing the pelitic-marly (pml0–2) and the pelitic-arenaceous (p-a) intervals (from UAS survey); b) the pml2 interval with the landslide detachment zone; c) lithic sandstones; d) the Ca key-horizon nearby the Corniolo village; e) strath terrace at about 540 m a.s.l. on the southern (right) bank of the Bidente River valley.

Buckling folds of layers are usually ascribed to DSGSD processes (e.g. Chigira, 1992; Jaboyedoff et al., 2013). Chevron-like folds were observed at different sites in the Corniolo and Verghereto areas on slope-parallel bedding surfaces, mainly at elevations between 750 and 800 m a.s.l.. They are developed over flatiron triangular facets (Fla–c in Figs. 1, 7), which have been shaped by differential erosion of the heterogeneous flysch sequence. Whereas pelitic beds have been strongly weathered (Fig. 8a), the sandstone layers also experienced fracturing and fragmentation (Fig. 8b). These processes reduced the rock mass strength and predisposed the rock layers to buckling phenomena driven by gravitational shear stress along 45°-dipping beds. Buckling features were also observed in the highermost sector of the Corniolo slope (FLa, see Fig. 8c) and in the Poggio Baldi area, at the base of the pml2 layer (Fig. 8e).

Other typical structures ascribable to DSGSD were trenches in which the rock mass was decomposed in disjointed blocks and the continuity of bedding was lost (Fig. 8d). On the Corniolo slope, trenches were concentrated in three levels at different elevations: between 680 and 750 m a.s.l. (lower level); around 900 m (middle level), where they were often paired with counterscarps, between 900 and 950 m (upper level), along the trace of the Th1 thrust surface (Fig. 7).

Minor landslides were present along the SE side of the Alpicella stream (Fig. 8f) and around the Piano d'Arcai tableland (Fig. 5h).

Table 1
Generations of fluvial terraces as recognised by Wegmann and Pazzaglia (2009). Corresponding terraces observed in the study area (I–III) are indicated, together with the classification of terraces for the Adriatic piedmont sector of the Apennines after Nesci et al. (2012).

Level Wegmann and Pazzaglia (2009)	Height above thalweg (middle sector of the Bidente River valley)	Level Nesci et al. *(2012)*	Height above thalweg *(study area)*	Elevation (this study, Fig. 8, 13)	Age
QT0	424 m	–	–	–	700 ± 900 ka
QT1	315 m	–	–	–	620 ± 30 ka
QT2	190 m	T1	140–150 m	*640 m(I)*	440 ± 50 ka
QT3	123 m	T2	–	–	140 ± 10 ka
QT4	67 m	T3	40–50 m	*530–540 m(II)*	28.4 ± 350 ka
QT5	43 m	T3	–	–	22.78 ± 200 ka
QT6	28 m	T3	10–20 m	*500–515m*(III)	13.03 ± 100 ka
QT7	21 m	T4	–	–	9.65 ± 110 ka
QT8	11 m	T4	–	–	6.41 ± 50 ka
QT9	<5 m	T4	–	–	1.93 ± 70 ka

Landslides reported in Fig. 3 on the Verghereto, Corniolo, and Capanne slopes were better identified as wide areas affected by shallow and complex movements involving both the bedrock and either colluvial and debris deposits. In these areas, morphological mid-slope terraces were recognised at different elevations.

Finally, different stream segments are affected by anomalous high gradient pointing at a stream network in disequilibrium conditions at both Corniolo and Poggio Baldi sites. Field work allowed the identification of knickpoints along both the main channel and its tributaries (Figs. 7, 8g). In the same area, Troiani et al. (2017), through spatial analysis at the regional scale of the stream length gradient (SL) index (Hack, 1973) detected a knickzone in the same valley sector (Fig. 7) and interpreted this stream anomaly as one of those connected to DSGSD. The use of the SL index for identifying and interpreting knickzones along stream networks was reported by Galve et al. (2014) and has been widely discussed in Troiani and Della Seta, 2008; Troiani et al. (2017).

4.3. Geomechanical data

The flysch deposits along the tributary Alpicella and Ritorno streams flanking the lower sector of the Corniolo slope were characterised in terms of the GSI value (Hoek and Brown, 1997) and following the chart by Marinos and Hoek (2001). Several GSI values were also estimated for outcrops in the uppermost sector of the slope and along the Th1 damaged zone. Points of GSI estimates are reported in Fig. 7, including the geomechanical classes a–g, indicating from good to poor-quality rock masses.

4.4. Original slope topography and aerial photogrammetry of the Poggio Baldi area

Slope restoration to the original topography prior to the first activation of the Poggio Baldi landslide in 1914 (Fig. 9a) was carried out by rectifying contour lines (Figs. 9b, b') of the topographic map dating back to 1998, which was prior to the 2010 failure event. The drainage network was reconstructed taking into account the following: i) a ditch once flowed in the area where today lies the landslide debris, which can be called the Poggio Baldi ditch (Fig. 9a); the Fosso dei Monti ditch deviated from the landslide body, thus its linearity needed to be restored; iii) similarly, the bed of the Bidente River, which during the various reactivations of the landslide has undergone a progressive southward migration, was brought back to its pre-landslide position.

A remote sensing survey (aerial photogrammetry) of the Poggio Baldi detachment and accumulation areas was carried out through a Phantom 4 APR UAS (unmanned aerial system), weighing 1380 g and equipped with a GPS/GLONASS receiver antenna, an integrated 12.4 Mpixel camera, and a field of view (FOV) of 94°. The point cloud of the entire area counted 88 million points (Fig. 9c), while the detachment area included 6.5 million points (Fig. 9d). First, a semi-quantitative analysis was completed using the Discontinuity Set Extractor (DSE) software (Riquelme et al., 2014) by running various calculation cycles with different densities of the point cloud (six sub-sampling with density varying from 258×10^3 to 2×10^6 points (Fig. 9d). Because DSE identifies joint systems based on the number of points on single discontinuity surfaces, to avoid neglecting the persistent discontinuities that were represented by a few joints on the point cloud, it was necessary to carry out a semi-manual analysis with the Coltop3D® software. Finally, using the Split-FX software, a manual control analysis was performed by combining two-dimensional images with the point cloud.

5. Data analysis and integration

Dip domain distribution along transects A–A' and B–B′ (Fig. 5a, f) shows a common geometric signature for the SW-dipping sedimentary multilayer, making the backbone on the Poggio Baldi and Corniolo slopes. Considering these data and the general NE vergence of the Apennine belt, a complex type of fault-propagation fold was reconstructed.

On the Poggio Baldi slope, the southern sector of the fold (Fig. 10a) was composed of: i) a wide, low-dipping backlimb sector (I); ii) a central zone with a kink-like type of folding (Fig. 5b) and several fold dip-panels (II-I-III); iii) a narrow core zone with an overturned forelimb (IV) hosting minor, short wavelength folds; and iv) a tight syncline structure in the easternmost sector (IV–V). The reconstructed geometry was mainly constrained to the trend of the Ca key-horizon, which crops out in the overturned dip-panel and in the eastern syncline. Along profile A–A', the Th1 and Th2 damaged zones were found at transitions between different dip-panels (Figs. 5a, 10a), and the type of tectonic deformation is consistent with the presence of breakthrough thrusts (Suppe and Medwedeff, 1990). Reverse faults were observed cutting through the overturned, sub-vertical fold forelimb with low-cut off angles (Fig. 5c and plot 1 in Fig. 10a), as a high-angle breakthrough geometry would require. The location of the syncline breakthrough thrust (Th2) was inferred considering the increased deformation, including cleavage S1 (Fig. 5e and plot 2 in Fig. 10a) and the position of the overturned forelimb/frontal syncline transition.

The reconstruction proposed for geological profile B–B′ is rather similar and outlined by the geometric attitude of the pml0–2 layers (Fig. 11a). East of the wide backlimb zone, the fault-propagation fold geometry was again presented, showing SW-dipping kink bands (II–I), a sub-horizontal dip-panel (III), an overturned forelimb (IV), and a forelimb syncline (V). Above 900 m of elevation, the vegetation covering the geological bedrock was thicker and more impenetrable than along profile A–A', thus the positions of the Th1 and Th2 breakthrough thrusts were inferred from the location of the damaged zone and dip domain distribution.

Geomorphological features ascribable to a DSGSD (Figs. 7, 8) were reported for both geological profiles. Along section B–B′ on the Corniolo slope, these elements were clustered within the hanging-wall block of the breakthrough thrust Th1, yet were absent within the overturned forelimb and the frontal syncline. Buckling folds on the Fla. flatiron

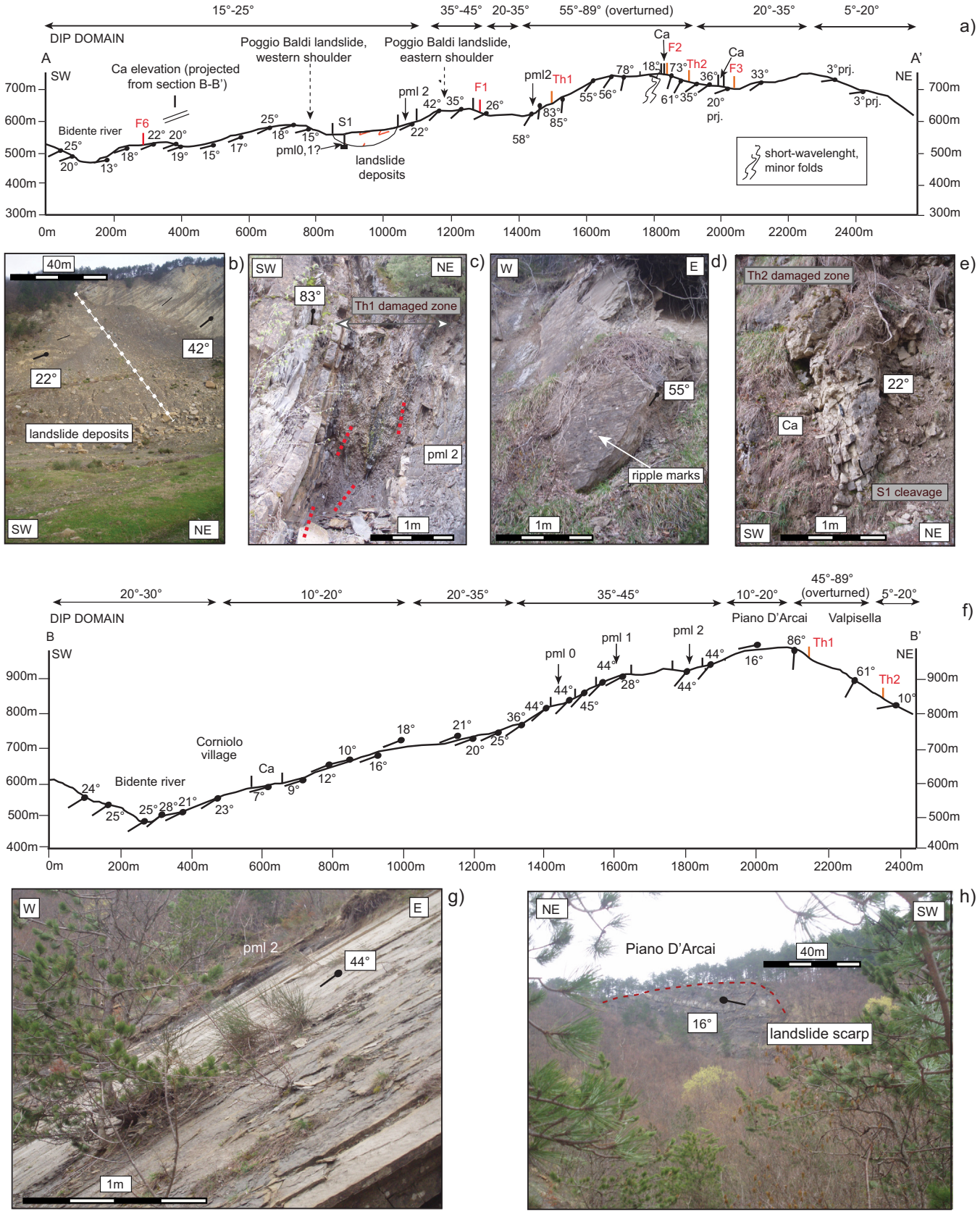

Fig. 5. a) Dip measurements and dip domain distribution along transect A–A' (trace in Fig. 3). Legend: Ca = Calanca layer; pml0–2 = pelitic-marly layers; Th1, Th2 = thrust and related damaged zones; F1–F6 = strike-slip faults; S1 = well (location in Fig. 3); b) kink-fold in the Poggio Baldi detachment area; c) reverse faults (dashed red lines) in the Th1 damaged zone; d) ripple marks on top of overturned beds; e) the Ca key-horizon disrupted by pervasive cleavage within the Th2 damaged zone; f) transect B–B'; g) slope-parallel beds in the upper Corniolo flatiron (Fla); and h) western edge of the Piano d'Arcai tableland with gently SW-dipping beds and a landslide scarp.

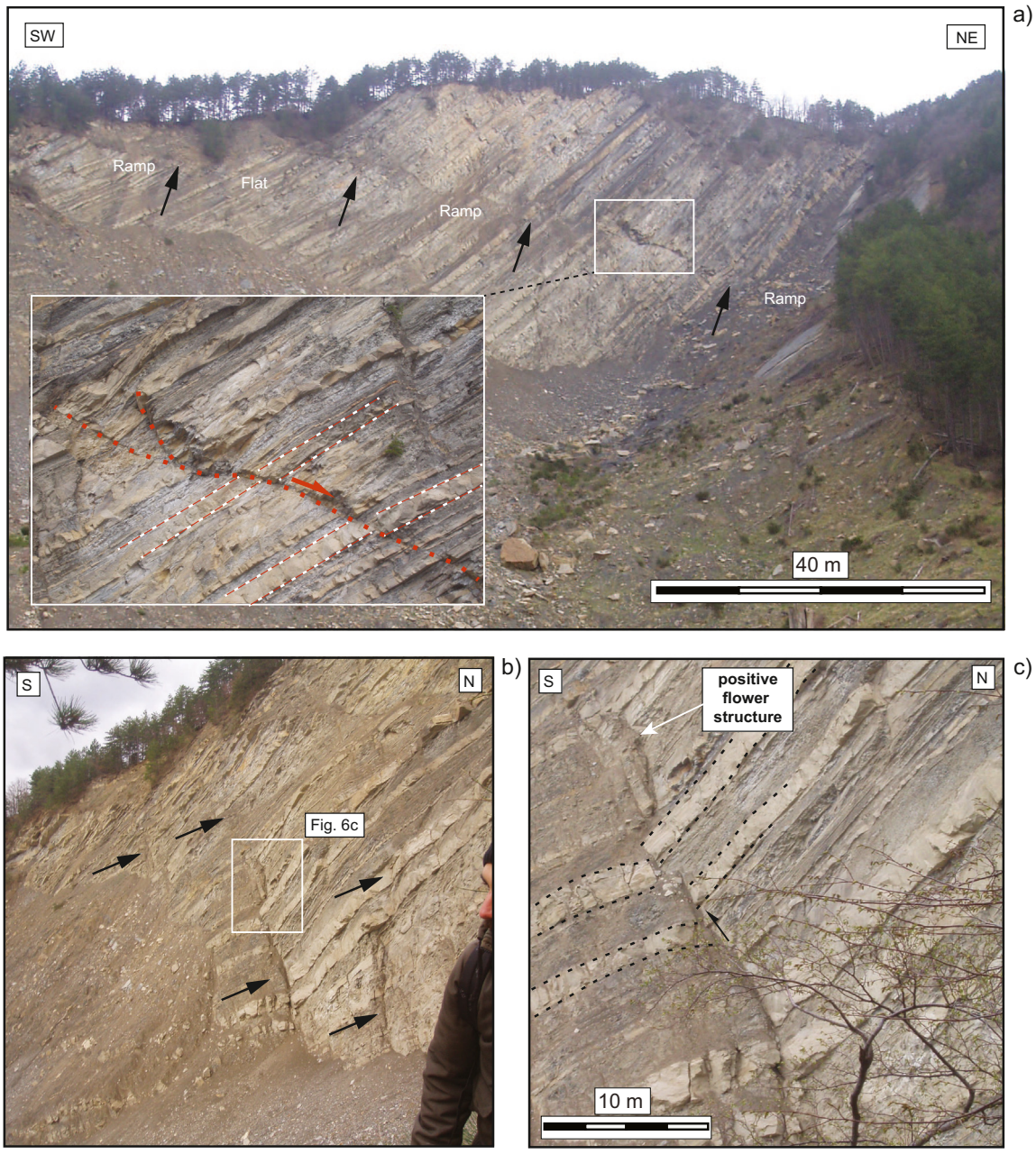

Fig. 6. Main tectonic features observed on the detachment area of the Poggio Baldi landslide: a) low-angle normal faults (LANF) with very-low displacement as evidenced in the lower-left box; b) set of NNE-SSW-oriented, sub-vertical faults; with c) transpressive kinematics and structures.

and the upper trench level were confined within the I kink panel in the hinge zone of the fold. Some trenches were also observed near the Th1 breakthrough thrust; the middle trench level and flatirons with buckling evidence (FLb, FLc) were found in the II kink panel in the fold backlimb. Finally, the lower trench level and shallow landslides were gathered in the lowermost kink panel I (Fig. 11a). Apart from landslides, the number of gravity-driven features was reduced along section A–A', and no elements were present in the foot-wall block of thrust Th1 (Fig. 10a). Trenches were present on the western shoulder of the detachment area, along the Th1 trace, and on the eastern side of the Poggio Baldi area (Fig. 7), where buckling was observed within the pml2 marly horizon (Fig. 8e).

Fig. 11b reports the results of GSI evaluation along the geotechnical section B–B*, partly corresponding to profile B–B′. GSI values were projected from outcrops found along the Alpicella and Ritorno erosive valleys on the western and eastern sides of the Corniolo slope, respectively (Fig. 7). The lowest GSI values (e, f) were concentrated in the eastern zone of profile B–B* where a highly-deformed, weakness zone with a counter-slope attitude, partly coinciding with a trench zone, was outlined. Downslope, the GSI values were good (a–c) except for few, isolated sites (e–g) delimiting a further smaller weakness zone. Further GSI values were estimated in the central and northern sectors of the study area, where good values prevailed (b) except in the narrow Th1 and Th2 deformation zone (Fig. 7).

Finally, the results of the automated structural analysis on UAS-derived point clouds of the Poggio Baldi detachment area (Figs. 9c, d) are summarized in Table 2. Main discontinuity systems, including bedding (S0 = J1) and ten joint sets, are shown on the stereoplot in Fig. 10b. The corresponding pole density plot in Fig. 10c provides evidence that the bedding was the main discontinuity system on the slope face

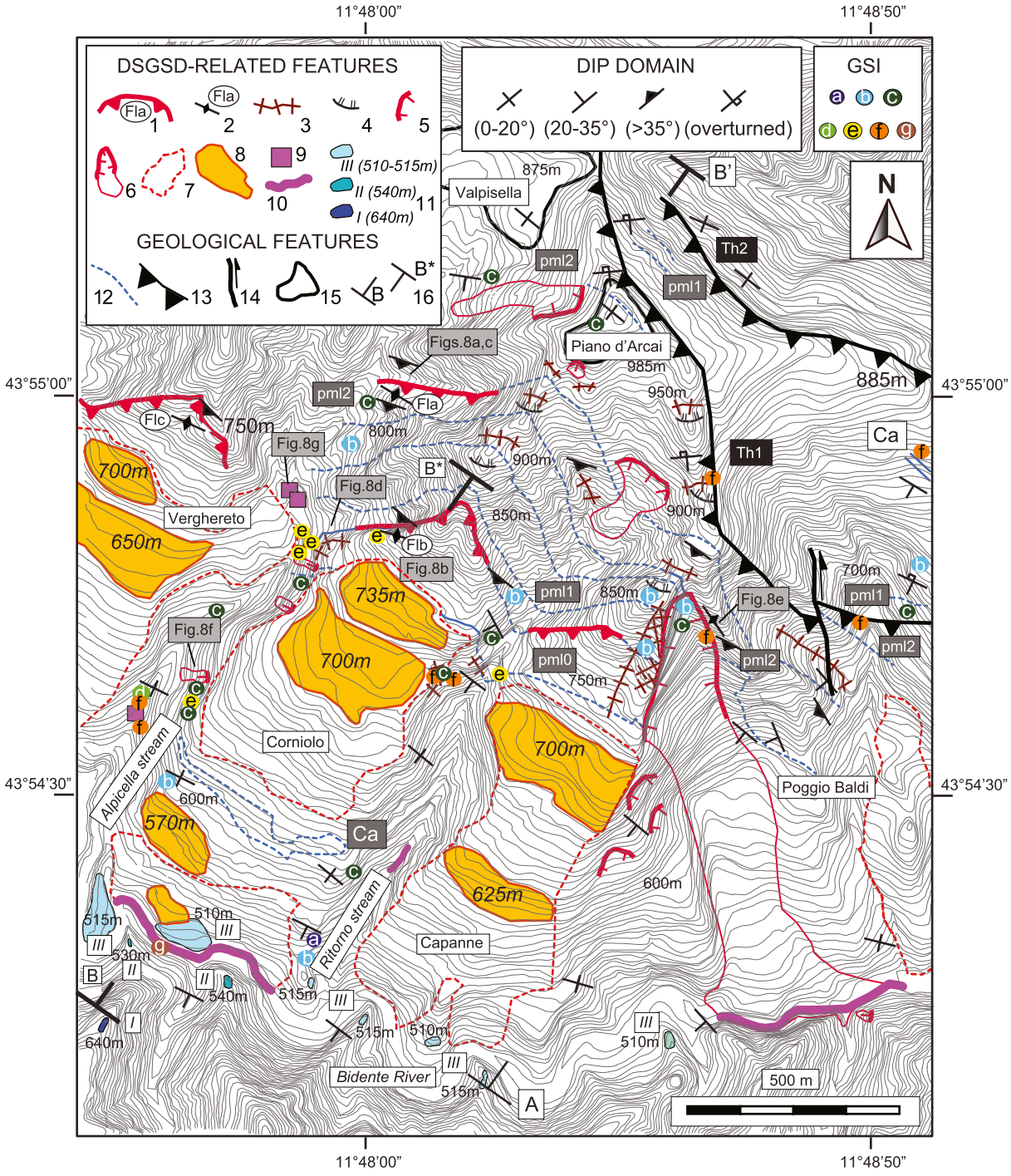

Fig. 7. Inventory map of DSGSD-related features. Main geological elements and measured GSI values with classes a–g, ranging from good to poor quality rock mass, are reported. Legend: 1) upper limit of DSGSDs along flatiron surfaces Fla-c; 2) buckling; 3) trench; 4) counter-scarp; 5) secondary scarp; 6) minor landslides; 7) area affected by large landslide redrawn from Fig. 3; 8) DSGSD-related morphological terrace; 9) knickpoint; 10) knickzone along the Bidente River valley; 11) fluvial terraces (I–III orders, see Table 1); 12) geological limits (Ca = 'Calanca' key-horizon; pml0, pml1, pml2 = pelitic-marly layers); 13) thrust; 14) strike-slip faults; 15) morphostructural surface; 16) trace of geotechnical profile B–B* (Fig. 11b).

and set J2 N108; 73° (dip direction; dip) as the prevalent joint system. The compatibility of discontinuity sets to different failure mechanisms was investigated using the Markland method (Markland, 1972) and considering the original topography of the rock slope before 1914 (Fig. 9b, b'), with a slope face = N150; 33°. Translational sliding movements of rock wedges result the unique compatible mechanism, allowed along intersection lines between: i) J1 = S0 and J6; ii) J1 = S0 and J3; iii) J3 and J6 (Fig. 11b).

6. Discussion

The architecture of the fault-propagation fold reconstructed in this work for the mountain ridges hosting the Poggio Baldi landslide is consistent with the dip domain distribution in the local flysch sequence and the presence of damaged zones Th1 and Th2. The fold geometry is constrained by outcrops of the 'Calanca' and pml0–2 key-horizons in the western half and core zones of geological profiles A–A' and B–B'

Fig. 8. DSGSD-related features: a) weathered pelitic bed in the Verghereto flatiron (Flc); b) fragmented sandstones layers in the lower Corniolo flatiron (Flb) with buckling evidence; c) buckling folds observed in the upper Corniolo flatiron (Fla); d) trench; e) buckling within the pml2 layer, the dashed white line indicates the fold axis; f) minor landslide, the dashed line marks the detachment area; and g) knick-point.

(Figs. 10a and 11a). The nucleation of the high-angle and syncline breakthrough thrusts implies the deformation of an original simple fault-propagation fold, with further folding, passive rotation of the backlimb dip-panels, and flattening of the core zone (Suppe and Medwedeff, 1990). This explains the presence of the II kink panel with 45°-inclined beds and the Piano d'Arcai and Valpisella morphostructural surfaces in the fold core where bedding is gently dipping (15–20°) (Fig. 11a).

DSGSD features are widespread over the Corniolo slope, but are also reported for the Verghereto, Capanne, and Poggio Baldi slopes (Fig. 7). Gravitational deformation is in an evident state of activity because it produces unaltered and unweathered geomorphological features: trenches without infilling materials (Fig. 8d), buckling folds (Figs. 8b, c, e), counter-scarps, active landslides on the edges of the DSGSD (Figs. 2a–d, 8f) and, finally, knickpoints (Fig. 8g) and knickzones (Fig. 7), which are representative of the imbalance of the river network. Geomorphological markers were not only found in the lower parts of the slopes, where shallow landslides, trenches, knickpoints, and knickzones are concentrated, but also in the highest slope sectors with a repeated pattern (trench/counterscarp-buckling). Evidence of

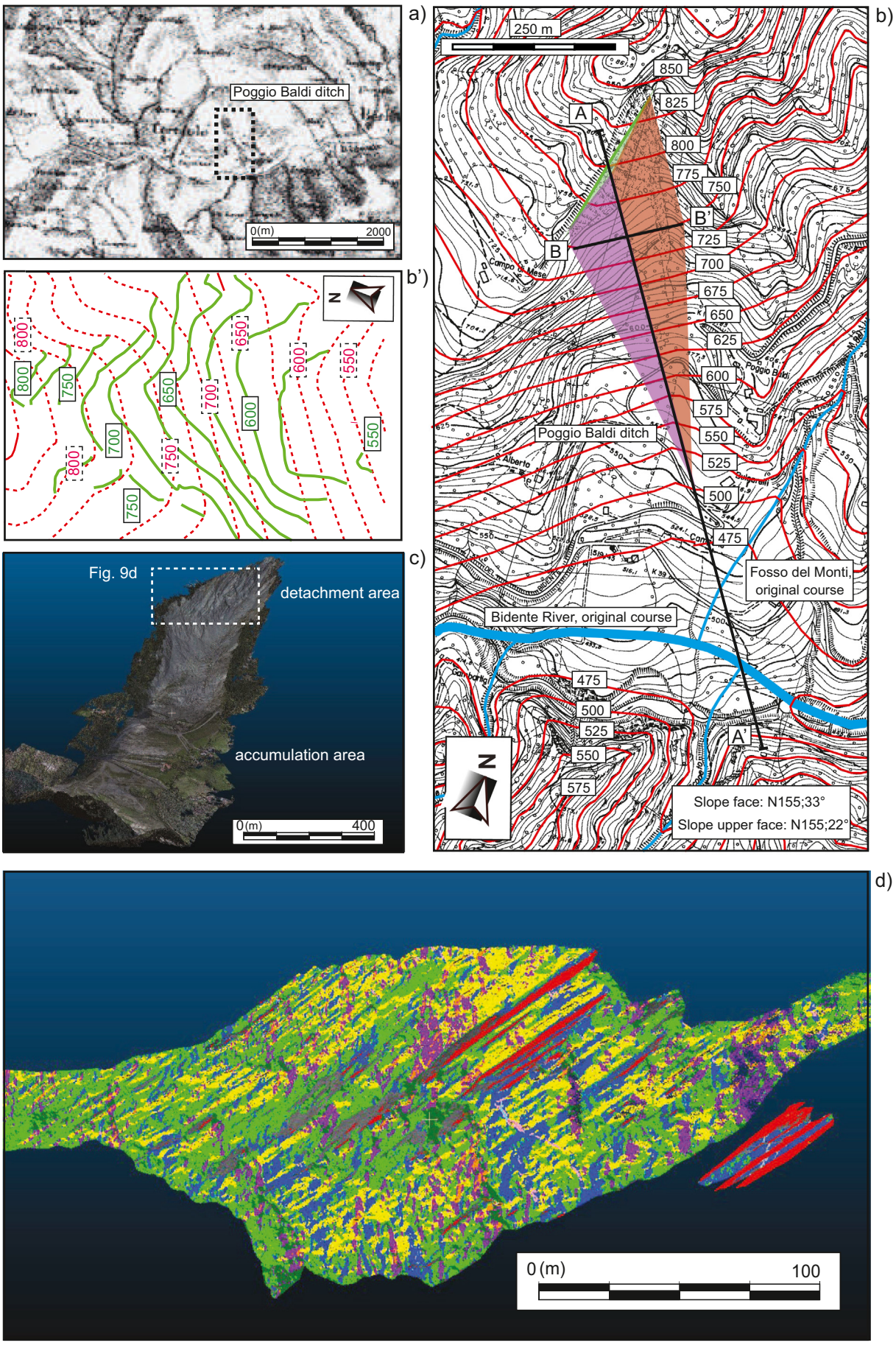
a)
Poggio Baldi ditch
0(m)
2000
b')
N
800
750
650
700
600
550
c)
Fig. 9d
detachment area
accumulation area
0(m)
400
b)
250 m
A
B
B'
A'
Poggio Baldi ditch
Fosso del Monti, original course
Bidente River, original course
Slope face: N155;33°
Slope upper face: N155;22°
d)
0 (m)
100

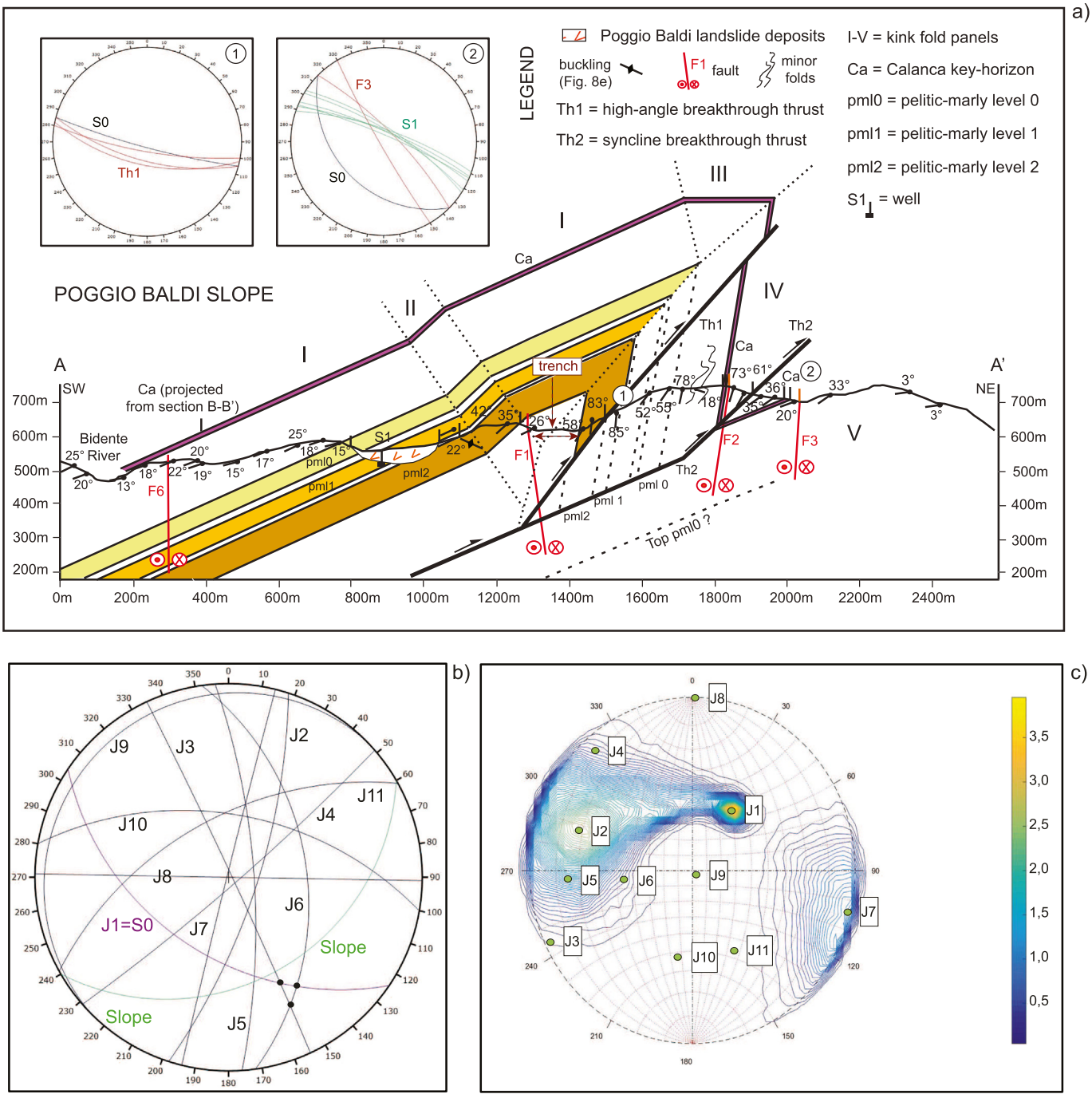

Fig. 10. a) Fold structure along profile A–A' (trace in Fig. 3). Dotted lines indicate kink axial surfaces, dashed lines the hypothesized extension of non-observed horizons according to geometric constraints. Structural plots at stations 1 and 2 (see Fig. 3) and DGSD features reported in Fig. 7 are shown; b) plot reporting discontinuity systems (including bedding S0) recognised trough automated analysis on the Poggio Baldi escarpment (Table 2) and possible wedge failures (black circles); c) pole density plot (contour lines each 1.25%).

buckling was observed on the flatiron surface Fla. at 830 m a.s.l. (Fig. 8c), while trenches, counter-scarps, and minor landslides (Fig. 5h) were found above 900 m a.s.l. around the Piano d'Arcai tableland and along the Th1 thrust (Fig. 7).

Geomorphological features ascribable to an active DSGSD are confined within the hanging-wall block of the high-angle breakthrough thrust Th1. This is probably mainly due in particular to the geometric setting of the fold and the overturned forelimb. Indeed, the eastern parts of the slopes (Figs. 10a, 11a) feature sub-vertical beds that may be more prone to localised toppling rather than to large-scale deformation, as observed in the backlimb zones.

Figs. 12 and 13 summarise the conceptual model of slope evolution inferred for the Corniolo slope. The inherited structural and lithological features are thought to be the main predisposing factors for DSGSD

Fig. 9. Historical map of the study area (1888) showing the Poggio Baldi ditch (within the dashed box); b) original topography before 1914 in red lines drawn over the 1:5000 scale raster map of the Emilia-Romagna region (1998). Red and purple areas indicate S0 and J6 surfaces, respectively. Traces of sections A–A' and B–B′ in Figs. 14a, b are indicated; b)' particular of the landslide detachment area with red, dashed lines of the original topography obtained by rectifying green lines of the 1998 topography; c) point cloud of the Poggio Baldi landslide from aerial photogrammetry; d) point cloud of the detachment area western shoulder with main discontinuity systems evidenced by different colours (see Table 2).

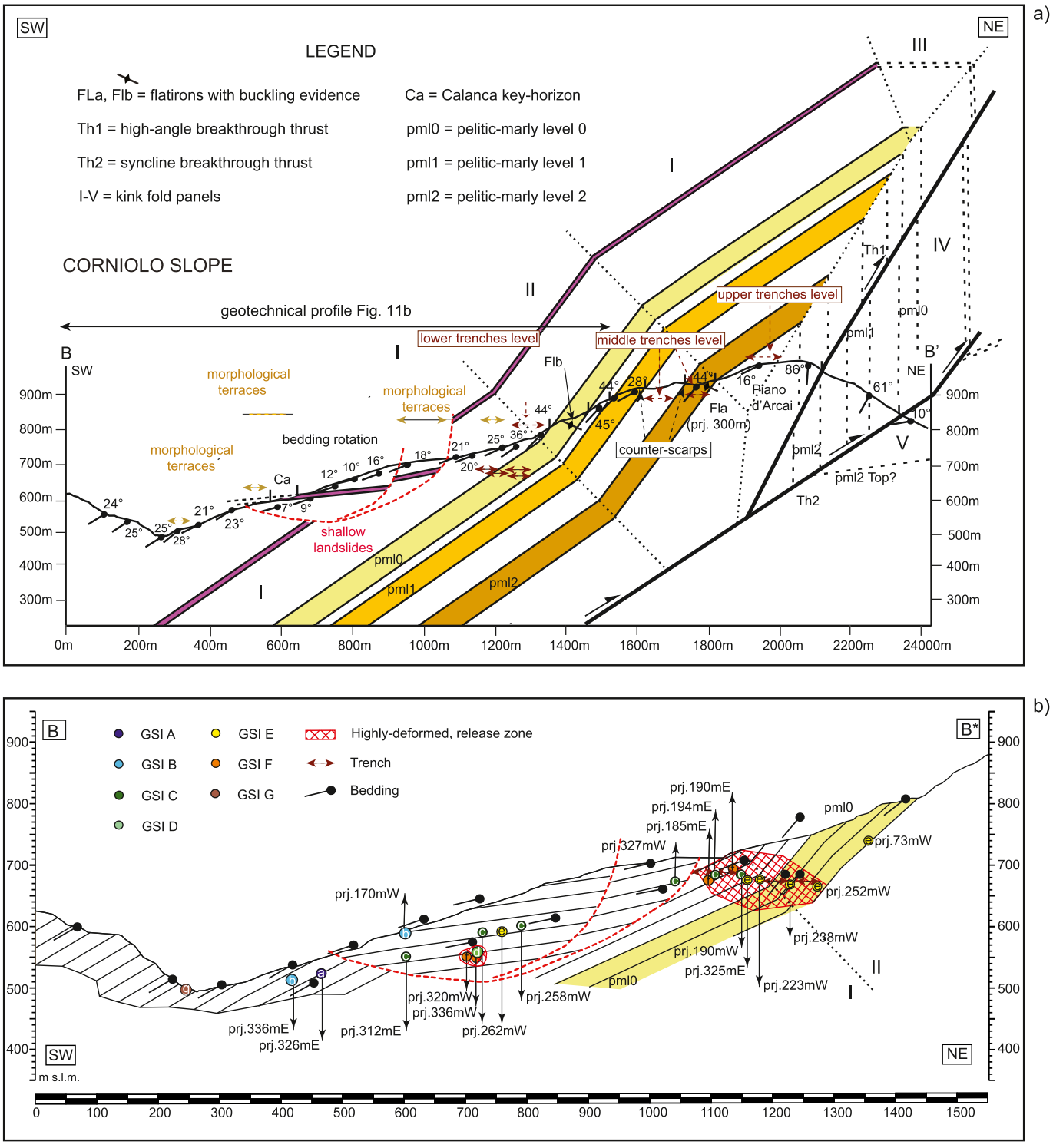

Fig. 11. a) Fold structure along profile B–B′ (trace in Fig. 3). Dotted lines indicate kink axial surfaces, dashed lines the hypothesized extension of unobserved horizons according to model constraints. Main DSGSD features as reported in Fig. 7 are shown; and b) geotechnical section of the Corniolo slope bearing GSI values projected from the Alpicella (western, W) and Ritorno (eastern, E) streams.

evelopment. The progressive incision of the Bidente River valley during the late Quaternary is argued to be the main long-term process driving the onset of DSGSDs and the evolution of the coupled slope–channel system, also according to the model proposed by Larsen and Montgomery (2012). As previously mentioned, an ongoing DSGSD process was already hypothesized by Troiani et al. (2017) due to the presence of a well-developed anomalous segment of the Bidente river longitudinal profile in this valley sector. Moreover, the longitudinal profile of the main watercourse presents a wide knickzone (Fig. 7), while a series of knickpoints occur along the local tributary streams (Fig. 8g). On the other hand, the preserved remnants of strath terrace levels confirm the long-term erosional trend and strong bedrock incision during the late Quaternary.

Starting from the spatial distribution of DSGSD features, the geostructural dataset, and the model of the long-term valley entrenchment, a first attempt for multi-step morphogenesis can be proposed.

Table 2
Discontinuity systems found through point cloud analysis by means of DSE, Coltop 3D and Split FX software.

Set	Dip dir.	Dip (°)	Pole density (%) (Fig. 13b)	Spacing (m)	Software		
					DSE	Coltop 3D	Split FX
J1 = S0	N214	46	35,189	6.13	x	x	x
J2	N108	73	26,368	6.01	x	x	x
J3	N65	88	0,0541	3.30		x	
J4	N139	85	0,2392	3.71		x	x
J5	N86	75	10,378	2.11		x	
J6	N82	46	0,2599	2.75		x	
J7	N284	89	0,7735	3.57	x		
J8	N181	90	0,0278	7.42	x		
J9	N315	4	0,0155	10.86	x		
J10	N10	54	0,0107	20.15	x	x	
J11	N331	56	0,0208	4.45	x	x	

Unfortunately, the lack of absolute dating for the strath terraces sequence prevents us from providing a well-constrained height-age model for estimating the long-term valley incision rates. Nonetheless, although the exact terrace chronology cannot be estimated, the position of the recognised terrace remnants along the valley sides suggests that the Bidente River headwaters experienced the same valley deepening phases, with the same relative chronology, already known for the main rivers draining the Adriatic piedmont area of the northern Apennines (Wegmann and Pazzaglia, 2009; Nesci et al., 2012).

In the first stage (I) of the Quaternary valley morphoevolution, dating back to the middle Pleistocene according to the first terrace level recognised in the study area (Table 1), the ancient valley floor was standing at about 640 m a.s.l. (i.e. I terrace level in Fig. 7), which would be 140–150 m above the present thalweg. Figs. 12a and 13a show the fold architecture in section and planimetric view at this stage, as derived from the Miocene multi-step tectonics. An original topography in Fig. 12a has been derived from the trend of the morphostructural elements and nullifying the effect of the subsequent lowering in areas characterised by trenches (Fig. 12a).

During the second stage (II), inferred from the Late Pleistocene time, after a prevalently vertical erosional phase, the ancient Bidente River laterally eroded to reach an elevation of about 530 m a.s.l. (i.e. II terrace level). This implied a lateral unconfinement, which determined the release of the entire geological structure and the onset of the first DSGSD (Fig. 12b). This developed over a basal weakness surface/zone coinciding in two locations as follows: i) in the upper sector with the 45°-dipping pml0 layer (at the transition between the II and I kink panels), and ii) with a newly generated surface in the lower slope sectors having a break-out geometry near the Bidente River. This hypothesis is supported by the distribution of gravity-driven features and GSI values. Trenches of the lower level, found between 680 and 750 m a.s.l. (Figs. 7, 11a), and the upper weakness zone identified by the lowest GSI values (Fig. 11b) are consistent with the tensile internal deformation at the head of the DSGSD (Fig. 12b). In addition, buckling processes were observed on the Flb and Flc flatirons within the pml0 horizon (Fig. 8b, c), evidence of bed-parallel sliding in response to gravitational stress in the apical zone. Therefore, the present-day flatiron surfaces found at about 800 m a.s.l. are considered as the upper boundary of the first DSGSD, which then developed in the area (Fig. 13b). The main deformation originating at stage II was therefore characterised by a biplanar compound geometry in its upper part, inherited by the fold setting (Fig. 12b), and then evolved into rotational sagging in the lower slope owing to the kinematic release of the newly generated break-out surface; this last can be traced following the position of the GSI-inferred lower weakness zone. Such a rotational effect could explain the activation of complex landslides, the morphological terraces, and the presence of the very low-dipping (5–20°) beds (Figs. 11a, b, 12b), which represent a gravity-driven anomaly (clockwise rotation) in the uppermost part of a cylindrical fault-propagation fold.

The last stage (III) of the valley morphoevolution consisted of the Bidente River entrenching down to reach the elevation of 510 m a.s.l., likely during the end of the late Pleistocene–early Holocene period. During this erosional stage, the combined effect of the further slope unconfinement and development of the former DSGSD since stage II would have caused the backward migration of the gravitational deformations. Trenches and counterscarps south of the Piano d'Arcai tableland and along the Th1 trace (Fig. 7) and the buckling evidence within the FLa flatiron (Fig. 8c) are attributed to this evolutionary step. Similar to stage II, the displacement surface/zone grew within a pelitic-marly horizon (pml2) and inside the kink panel II, where bedding is 45°-inclined, and had to be in part newly generated obliquely to the bedding (Fig. 12c). An extension to the north of the process, up to the thrust zone Th1, may also be hypothesized considering the Th1 damaged zone (Fig. 5c) along which GSI values are relatively low (Fig. 7) as a metric-wide, reactivated basal shear zone.

From the conceptual model illustrated in Figs. 12a–c and 13a–c, the pml0 and pml2 marly levels acted as preferential basal levels for gravity-driven deformations. This occurred because of their relatively low strength characteristics. The peak and residual friction angles $\varphi = 15°$ and $\varphi r = 13°$, respectively, and a cohesion of 0–2 MPa was determined by Oberti et al. (1986) for bedding planes within these lithologies along the Bidente River, a few kilometres southeast of the study area.

The geometry of the basal surfaces/zones separating the deforming rock volumes and the stable part of the fold structure resembles compound and rotational types of sagging (Hutchinson, 1988) in the higher and lower parts of the Corniolo slope, respectively. During the evolutionary stage (II), the deforming mass in the lower slope sector was displaced along an essentially circular, newly generated surface with toe break geometry (Fig. 12b). Except in the rear zone where trenches are clustered, no internal deformation developed, as is confirmed by the absence of counterscarps and middle-slope trenches below 700 m a.s.l. (Fig. 13b). Otherwise, the control of inherited structural features on gravity-driven deformation is clear in the rear zone. Here, buckling folds on the Flb and Flc flatirons, which are related to gravity-driven shear stress on bedding planes, were observed at the transition between the I and II kink panels, where bedding is rotated to a 45° dip value. A biplanar surface/zone developed following the fold geometry and joining the circular surface below (Fig. 12b).

On the contrary, during stage III, mass movements occurred only along the biplanar surfaces, coinciding in their upper parts to the base of the pml2 horizon and the Th1 damaged zone. According to Hutchinson (1988), a compound, noncircular sagging requires non-negligible internal deformation of the rock mass, as revealed by high-angle shear surfaces at the rearward parts and trenches/counterscarps in the middle slope sectors (Fig. 13c). These last features originate gravitational grabens and are not associated with any rotational component; unlike the DSGSD at stage (II), a circular basal surface was therefore excluded (Fig. 12c).

Along profile A–A' (Fig. 10a), and more generally on the Poggio-Baldi and Capanne slopes, DSGSD elements are fewer than on the Corniolo ridge. In addition, trenches on the western shoulder of the Poggio Baldi landslide show a trend parallel to the slope escarpment (Fig. 7); therefore, they could be linked to post-failure conditions. Likely, the first landslide event in 1914 cancelled most of the evidence for gravity-driven deformations. However, the conceptual model illustrated in Fig. 12 can also be applied to the Poggio Baldi area. The apical zone of the 1914 rock slide lies within the II fold panel, where bedding is 45° SW-dipping and part of the detachment surface is identified few metres above the pml2 lower limit (Figs. 4a, b). The buckling evidence at the base of the same stratigraphic level (Fig. 8e) and trenches right behind the landslide eastern shoulder (Figs. 7 and 11a) depict a deformation scenario rather similar to that illustrated in Fig. 12c for stage III of deformation on the Corniolo slope. Therefore, it can be hypothesized that the

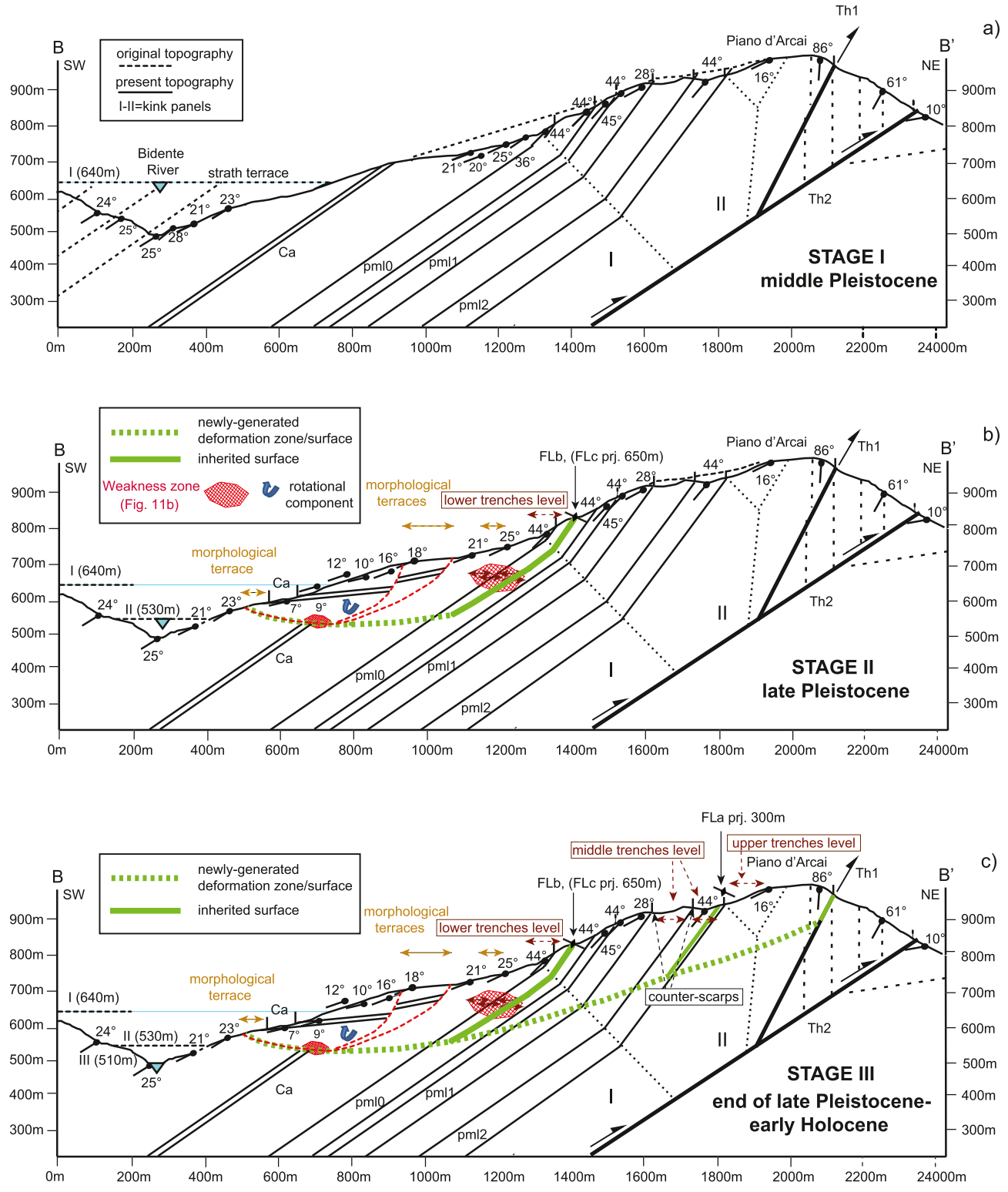

Fig. 12. (a–c) Three-step conceptual morphoevolutive model illustrating the onset and development of DSGSDs in the Corniolo valley side as a response to the late Quaternary bedrock river incision and slope unconfinement.

original rock-slide occurred in the context of an ongoing DSGSD (Fig. 13c), triggered by the upslope migration of the Poggio Baldi ditch (Fig. 9a), driven by progressive incision of the Bidente River course.

Finally, the reconstruction of the original slope topography (Figs. 9b, b') combined with the results of the photogrammetric and kinematic analyses performed on the detachment area (Figs. 9c, d and Table 2) and observations on the macro-structural elements (Figs. 6a–c) allowed the reconstruction of the geometry and volume of the rock wedge that detached in 1914 (Fig. 14). Among the possible discontinuity combinations compatible with a rock wedge sliding the one including S0 and J6 respect the geological constraints (Figs. 4a, b) and the results of the quantitative estimate of the fallen rock volume. In the longitudinal cross-section of the original slope (Fig. 14a), the sub-vertical transpressive faults observed on the main escarpment (Figs. 6b, c)

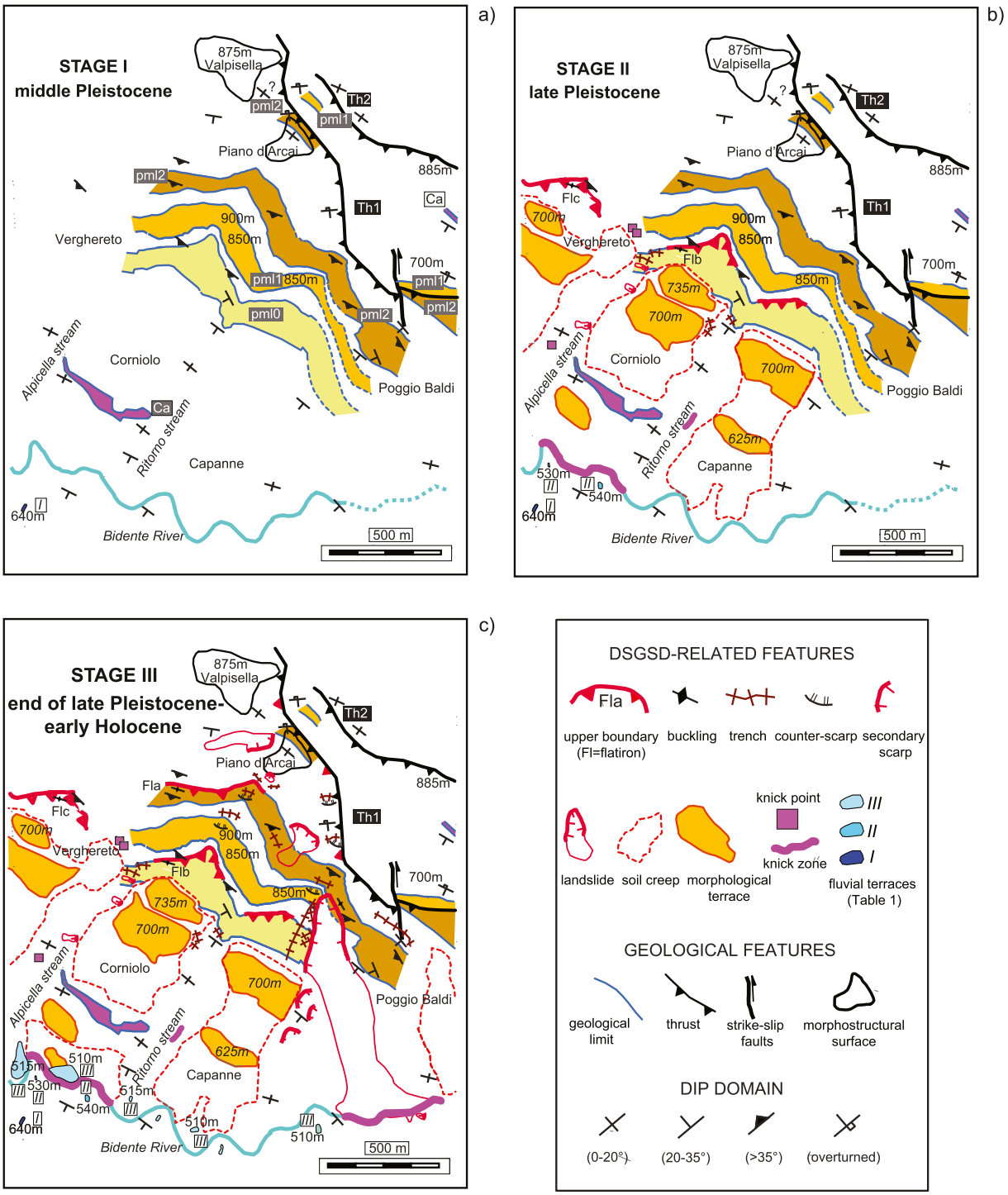

Fig. 13. (a–c) Planimetric views of the three-step DSGSD reconstruction shown in Figs. 12a–c.

play the role of rear tension cracks; their orientation (NNE-SSW) is compatible with the geometric attitude of the prevalent discontinuity systems J2 (and J7). Any particular meaning in terms of rock slope failures seems to be attributable to the LANF, apart from a possible wedge breakage along this persistent mechanical discontinuity during the 1914 collapse event (Fig. 14a). The transverse cross-section of the rock wedge shows a wedge opening angle $\gamma = 108°$ (Fig. 14b), while the reconstructed three-dimensional geometric model (Fig. 14c) outlines a rock volume of approximately 1.4×10^6 m^3. The other wedge combinations (S0 and J3, J3, and J6) brought volumes ranging from 0.58×10^6 to 0.72×10^6 m^3, remarkably lower than the volume of the mobilised material in the present landslide accumulation area (around 4.0×10^6 m^3, considering also the 2010 remobilisation event).

7. Conclusions

The mountain ridges hosting the Poggio Baldi landslide in the Northern Apennines are characterised by evidence of deep-seated gravitational slope deformation (DSGSD) including trenches, scarps and counterscarps, buckling, and minor landslides. These geomorphological elements are particularly evident on the Corniolo slope, west of the landslide area.

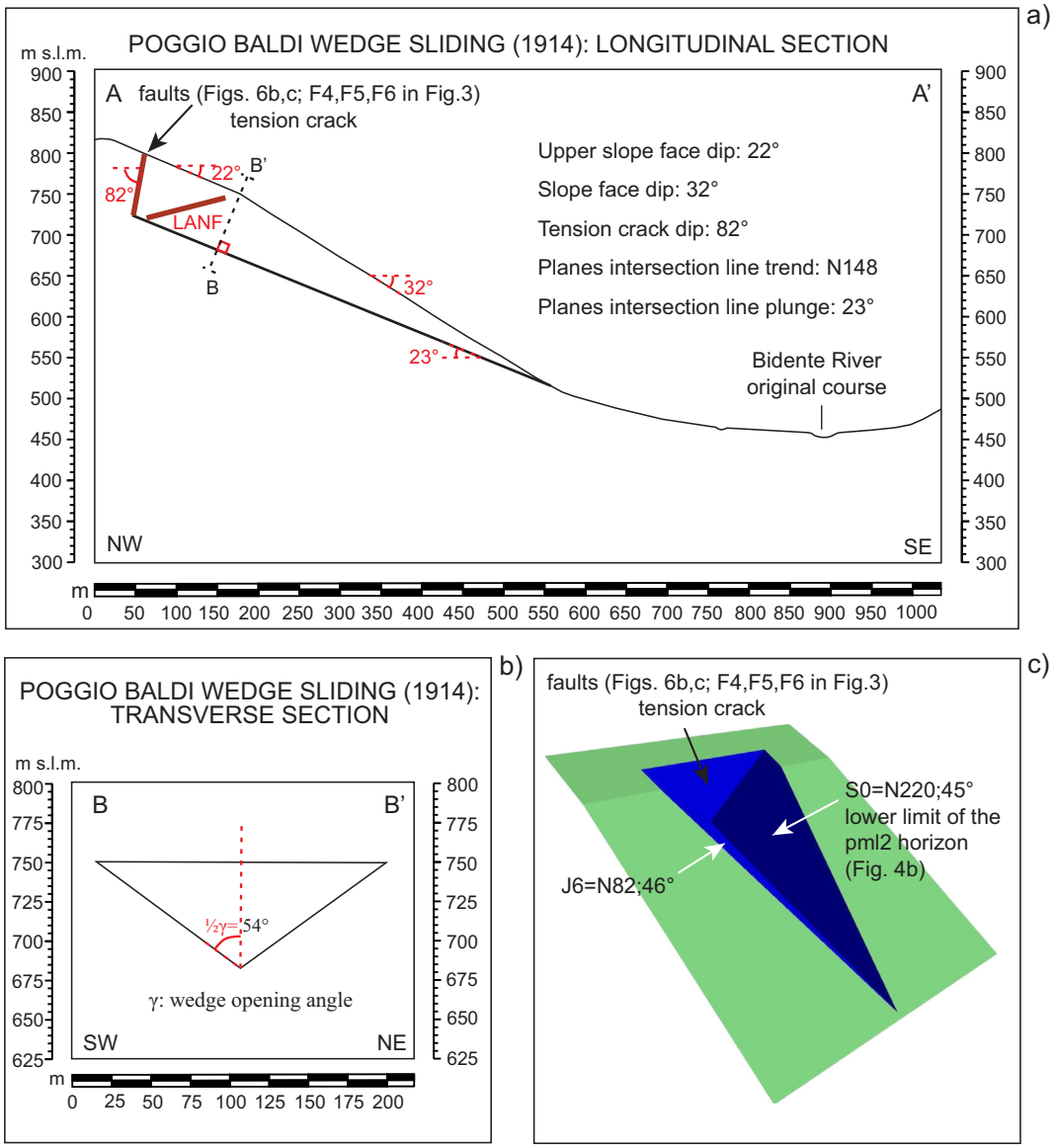

Fig. 14. a) Longitudinal section A–A' of the rock wedge along the intersection line of discontinuities J6 (N82; 46°) and S0 (N220; 46°); the main transpressive faults and the counter-slope dipping LANF recognised on the slope edge (Figs. 6a–c) are drawn. Transverse section B–B′ of the rock wedge, orthogonal to the sliding direction (N148; 23°). Traces of sections A–A' and B–B′ are reported in Fig. 9b; c) three-dimensional 3D geometric reconstruction of the rock wedge determined by discontinuities S0, J6 and the tension crack.

Dip domain data collected within the local Miocene flysch sequence outlined a complex geometry of the sedimentary multilayer that was reconstructed according to a model of fault-propagation folding. The structural setting of the fold was completed by the development of breakthrough thrusts whose formation implied a progressive, further kinking of the backlimb zone. This structural inheritance influenced the onset and development of a wide, multi-step DSGSD process, which is confined in the hanging-wall block of the upper breakthrough thrust. The gravitational deformation of the folded backlimb was also conditioned by the anisotropic behaviour of the heterogeneous siliciclastic deposits, featuring three pelitic-marly levels inter-layered with arenaceous horizons.

In the context of an active uplifting mountain chain, within a well-connected slope-channel system, the long-term bedrock incision of the Bidente River is hypothesized as the driving force for the onset of the DSGSD within the fold structure. This hypothesis is supported by the presence of a wide knickzone along the analysed portion of the river channel, a series of knickpoints along the main tributaries and three strath terrace levels, middle Pleistocene-to-early Holocene in age, hanging at different heights along the valley sides.

The conceptual model of DSGSD includes three stages following the progressive entrenchment of the Bidente River valley, which determined the slope lateral unconfinement and consequential mass movements with a backward evolution. These have occurred over displacement surfaces/zones partly inherited from structural levels and newly generated. Their geometries and the distribution of DSGSD-related features suggest a transition from a mainly rotational to a bi-planar compound sagging during the time evolution of the DSGSD process.

The model reconstructed for the Corniolo slope can be applied to the close Poggio Baldi slope, considering the similar pattern of geomorphological features ascribable to gravity-driven deformations. Therefore, the massive rock slope failure that occurred in 1914, with the detachment and mobilisation of a 1.4×10^6 m^3 rock wedge, can be framed in the context of an active DSGD process.

Declaration of competing interest

The authors declare that they have no known competing financial interests or personal relationships that could have appeared to influence the work reported in this paper.

Acknowledgments

The Authors are grateful to professors Gabriele Scarascia-Mugnozza, Salvatore Martino, Domenico Guida and Salvatore Piro for their support to scientific research in the Poggio Baldi area and to Dr. Leonardo Di Michele for his help during field surveys. Special thanks go to an anonymous reviewer whose criticisms and suggestions have improved the quality of the paper. This work was financially supported by Nhazca (CEO Paolo Mazzanti) and the research project "Integrated analysis and hazard-oriented modelling of large-scale slope instabilities featured by Mass Rock Creep" - prot. RG11916B88FA477F (PI Carlo Esposito) funded by "Sapienza" University of Rome.

References

Agliardi, F., Crosta, G., Zanchi, A., 2001. Structural constraints on deep-seated slope deformation kinematics. Eng. Geol. 59, 83–102. https://doi.org/10.1016/S0013-7952(00)00066-1.

Agliardi, F., Zanchi, A., Crosta, G., 2009. Tectonic vs gravitational morphostructures in the Central Italian Alps: constraints on the recent evolution of the mountain range. Tectonophysics 474, 250–270. https://doi.org/10.1016/j.tecto.2009.02.019.

Alfaro, P., Delgado, J., Esposito, C., Tortosa, F.G., Marmoni, G.M., Martino, S., 2019. Time-dependent modelling of a mountain front retreat due to a fold-to-fault controlled lateral spreading. Tectonophysics 773, 228233. https://doi.org/10.1016/j.tecto.2019.2282.

Ambrosi, C., Crosta, G., 2006. Large sackung along major tectonic features in the Central Italian Alps. Eng. Geol. 83, 183–200. https://doi.org/10.1016/j.enggeo.2005.06.031.

Argnani, A., Barbacini, G., Bernini, M., Camurri, F., Ghielmi, M., Papani, G., Rizzini, F., Rogledi, S., Torelli, L., 2003. Gravity tectonics driven by Quaternary uplift in the Northern Apennines: insights from the La Spezia-Reggio Emilia geo-transect. Quat. Int. 101, 13–26. https://doi.org/10.1016/S1040-6182(02)00088-5.

Badger, T.C., 2002. Fracturing within anticlines and its kinematic control on slope stability. Environ. Eng. Geosci. 8, 19–33. https://doi.org/10.2113/gsee.geosci.8.1.19.

Benini, A., Farabegoli, E., 1990. Tettonica trasversale nell'Appennino forlivese. La Linea del Bidente. Mem. Descr. Carta Geol. d'It. 46, 245–255.

Benini, A., Farabegoli, E., Martelli, L.E., Severi, P., 1991. Stratigrafia e paleogeografia del Gruppo di S. Sofia (alto Appennino Forlivese). Mem. Descr. Carta Geol. It. 46, 231–243.

Benini, A., Biavati, G., Generali, M., Pizziolo, M., 2012. The Poggio Baldi Landslide (High Bidente Valley): Event and Post-event Analysis and Geological Characterization. Proc. 7th EUREGEO - EUropean Congress on REgional GEOscientific Cartography and Information Systems. Bologna, Italy, pp. 64–65.

Bianchi Fasani, G., Di Luzio, E., Esposito, C., Martino, S., Scarascia-Mugnozza, G., 2011. Numerical modelling of Plio-Quaternary slope evolution based on geological constraints: a case study from the Caramanico Valley (Central Apennines, Italy). Geol. Soc. Lond., Spec. Publ. 351, 201–214. https://doi.org/10.1144/SP351.11.

Bianchi Fasani, G., Di Luzio, E., Esposito, C., Evans, S.G., Scarascia-Mugnozza, G., 2014. Quaternary, catastrophic rock avalanches in the Central Apennines (Italy): relationships with inherited tectonic features, gravity-driven deformations and the geodynamic frame. Geomorphology 21, 22–42. https://doi.org/10.1016/j.geomorph.2013.12.027.

Brideau, M.A., Yan, M., Stead, D., 2009. The role of tectonic damage and brittle rock fracture in the development of large rock slope failures. Geomorphology 103, 30–49. https://doi.org/10.1016/j.geomorph.2008.04.010.

Chalupa, V., Panek, T., Taborik P., Klimes, J., Hartvich, Grygar, R., 2018. Deep-seated gravitational slope deformations controlled by the structure of flysch nappe outliers: insights from large-scale electrical resistivity tomography survey and LiDAR mapping. Geomorphology 321, 174-187. doi:10.1016/j.geomorph.2018.08.029.

Chigira, M, 1992. Long-term gravitational deformation of rocks by mass rock creep. Eng. Geol. 32(3), 157–184.

Coquin, J., Mercier, D., Bourgeois, O., Feuillet, T., Decaulne, A., 2016. Is gravitational spreading a precursor for the Stífluhólar landslide (Skagafjörður, Northern Iceland)? Géomorphologie: relief, processus, environnement 22 (1), 9–24. https://doi.org/10.4000/geomorphologie.11295.

De Luca, G., Cattaneo, M., Monachesi, M., Amato, A., 2009. Seismicity in Central and Northern Apennines integrating the Italian national and regional networks. Tectonophysics 476, 121–135. https://doi.org/10.1016/j.tecto.2008.11.032.

Della Seta, M., Esposito, C., Marmoni, G.M., Martino, S., Scarascia-Mugnozza, G., Troiani, F., 2017. Morpho-structural evolution of the valley-slope systems and related implications on slope-scale gravitational processes: new results from the Mt. Genzana case history (Central Apennines). Geomorphology 289, 60–77. https://doi.org/10.1016/j.geomorph.2016.07.003.

Di Luzio, E., Saroli, M., Esposito, C., Bianchi-Fasani, G., Cavinato, G.P., Scarascia-Mugnozza, G., 2004a. The influence of inherited structural framework on deep-seated gravity deformation phenomena: the fault-bounded Majella anticline (central Apennines, Italy). Geomorphology 60, 417–432. https://doi.org/10.1016/j.geomorph.2003.10.004.

Di Luzio, E., Bianchi-Fasani, G., Saroli, M., Esposito, C., Cavinato, G.P., Scarascia-Mugnozza, G., 2004b. Massive rock slope failure in the central Apennines (Italy): the case of the Campo di Giove rock avalanche. Bullettin of Engineering Geology and the Environment 63, 1–12. https://doi.org/10.1007/s10064-003-0212-7.

Di Naccio, D., Kastelic, V., Carafa, M.M.C., Esposito, C., Milillo, P., Di Lorenzo, C., 2019. Gravity versus Tectonics: the Case of 2016 Amatrice and Norcia (Central Italy) earthquakes surface coseismic fractures. Journal of Geophysical Research: Earth Surface 124, 994–1017. https://doi.org/10.1029/2018JF004762.

Discenza, M.E., Esposito, C., Martino, S., Petitta, M., Prestininzi, A., Scarascia Mugnozza, G., 2011. The gravitational slope deformation of Mt. Rocchetta ridge (central Apennines, Italy): geological-evolutionary model and numerical analysis. Bullettin Engineering Geology and the Environment 70 (4), 559–575. https://doi.org/10.1007/s10064-010-0342-7.

Dramis, F., Sorriso-Valvo, M., 1994. Deep-seated gravitational slope deformations, related landslides and tectonics. Eng. Geol. 38, 231–243.

Esposito, C., Martino, S., Scarascia-Mugnozza, G., 2007. Mountain slope deformations along thrust fronts in jointed limestone: an equivalent continuum modelling approach. Geomorphology 90, 55–72. https://doi.org/10.1016/j.geomorph.2007.01.017.

Esposito, C., Bianchi-Fasani, G., Martino, S., Scarascia-Mugnozza, G., 2013. Quaternary gravitational morpho-genesis of Central Apennines (Italy): Insights from the Mt. Genzana case history. Tectonophysics 605, 96–103. https://doi.org/10.1016/j.tecto.2013.06.023.

Esposito, C., Di Luzio, E., Scarascia-Mugnozza, G., Bianchi Fasani, G., 2014. Mutual interactions between slope-scale gravitational processes and morpho-structural evolution of central Apennines (Italy): review of some selected case histories. Rendiconti Lincei. Scienze fisiche e naturali 25. https://doi.org/10.1007/s12210-014-0348-3 (161-155).

Farabegoli, E., Benini, A., Martelli, L., Orevoli, G., Severi, P., 1991. Geologia dell'Appennino romagnolo da Campigna a Cesenatico. Mem. Descr. Carta Geol. d'It. 46, 165–184.

Galadini, F., 2006. Quaternary tectonics and large-scale gravitational deformations with evidence of rock-slide displacements in the Central Apennines (Central Italy). Geomorphology 82, 201–228. https://doi.org/10.1016/j.geomorph.2006.05.003.

Galve, J.P., Piacentini, D., Troiani, F., Della Seta, M. (2014). Stream Length-Gradient Index mapping as a tool for landslide identification, in Pardo-Igúzquiza, E., Guardiola-Albert, C., Heredia, J., Moreno-Merino, L., Durán, J.J., Vargas-Guzmán, J.A., (Eds.), Mathematics of Planet Earth. Lecture Notes in Earth Sciences, Springer-Verlag, Berlin Heideberg, 343–346. https://doi.org/10.1007/978-3-642-32408-6_155.

Gori, S., Falcucci, E., Dramis, F., Galadini, F., Galli, P., Giaccio, B., Messina, P., Pizzi, A., Sposato, A., Cosentino, D., 2014. Deep-seated gravitational slope deformation, large-scale rock failure, and active normal faulting along Mt. Morrone (Sulmona basin, Central Italy): Geomorphological and paleoseismological analyses. Geomorphology 208, 88–101. https://doi.org/10.1016/j.geomorph.2013.11.017.

Hack, J.T., 1973. Stream-profile analysis and stream-gradient index. U.S. Geological Survey Journal of Research 1, 421–429.

Hoek, E., Brown, E.T., 1997. Practical estimates of rock mass strength. Int. J. Rock Mech. Min. Sci. 34, 1165–1186.

Humair, F., Pedrazzini, A., Epard, J.L., Froese, C.R., Jabedoyff, M., 2013. Structural characterization of Turtle Mountain anticline (Alberta, Canada) and impact on rock slope failure. Tectonophysics 605, 133–148. https://doi.org/10.1016/j.tecto.2013.04.029.

Hungr, O., Leroueil, S., Picarelli, L., 2014. The Varnes classification of landslide types, an update. Landslides 11, 167–194. https://doi.org/10.1007/s10346-013-0436-y.

Hutchinson, J.N., 1988. General report: morphological and geotechnical parameters of landslides in relation to geology and hydrogeology, in: Bonnard, C., (Ed.), Landslides. Balkema, Rotterdam 1, 3–36.

Jaboyedoff, M., Penna, I., Pedrazzini, A., Baroň, I., Crosta, G.B., 2013. An introductory review on gravitational-deformation induced structures, fabrics and modeling. 605:1-12. Tectonophysics 605, 1–12. https://doi.org/10.1016/j.tecto.2013.06.027.

Kellog, K.S., 2001. Tectonic controls on large landslide complex: Williams Fork Mountains near Dillon, Colorado. Geomorphology 41, 355–368. https://doi.org/10.1016/S0169-555X(01)00067-8.

Larsen, I.J., Montgomery, D.R., 2012. Landslide erosion coupled to tectonics and river incision. Nat. Geosci. 5 (7), 468–473.

Marinos, P., Hoek, E., 2001. Estimating the geotechnical properties of heterogeneous rock masses such as flysch. Bull. Eng. Geol. Environ. 60, 85–92. https://doi.org/10.1007/s10064000009.

Markland, J.T., 1972. A useful technique for estimating the stability of rock slopes when the rigid wedge sliding type of failure is expected. Imperial College Rock Mechanics, Research Report 19 (10pp).

Martelli, L., Farabegoli, E., De Donatis, M., Severi, P., Benini, A., Mattioli, A., Pizziolo, M., Pignone, R., Catanzariti, R., Fornaciari, E., Spadafora, E., 2002. Carta geologica d'Italia. Scala. 1: 50000, Foglio. n. Bagno di Romagna. Servizio Geologico d'Italia, Selca, Firenze, p. 265.

Martelli, L., Santulin, M., Sani, F., Tamaro, A., Bonini, M., Rebez, A., Corti, G., Slejko, D., 2017. Seismic hazard of the Northern Apennines based on 3D seismic sources. J. Seismol. 21 (1), 1–25. https://doi.org/10.1007/s10950-017-9665-1.

Massironi, M., Genevois, R., Floris, M., Stefani, M., 2011. Influence of the antiformal setting on the kinematics of a large mass movement: the Passo Vallaccia, eastern Italian Alps. Bull. Eng. Geol. Environ. 70, 497–506. https://doi.org/10.1007/s10064-010-0340-9.

Mazzanti, P., Bozzano, F., Brunetti, A., Caporossi, P., Esposito, C., Scarascia-Mugnozza, G., 2017. Experimental landslide monitoring site of Poggio Baldi landslide (Santa Sofia, N-Apennine, Italy). 4th World Landslide Forum, Ljubljana Slovenia. In: Mikoš, M., Vilímek, V., Yin, Y., Sassa, K. (Eds.), Advancing Culture of Living with Landslides. Springer International Publishing, pp. 259–266 https://doi.org/10.1007/978-3-319-53487-9_29.

Mitra, S., 1990. Fault-propagation folds: geometry, kinematic evolution, and hydrocarbon traps. Amer. Ass. of Petrol. Geol. Bullettin 74, 921–945.

Moro, M., Saroli, M., Gori, S., Falcucci, E., Galadini, F., Messina, P., 2012. The interaction between active normal faulting and large scale gravitational mass movements revealed by paleoseismological techniques: a case study from central Italy. Geomorphology 151, 164–174. https://doi.org/10.1016/j.geomorph.2012.01.026.

Němčok, A., 1972. Gravitational slope deformation in high mountains. Proc. 24th International Geological Congress. Montreal, Canada 13, 132–141.

Nesci, O., Savelli, D., Troiani, F., 2012. Types and development of stream terraces in the Marche Apennines (central Italy): a review and remarks on recent appraisals. Géomorphologie: relief, processus, environnement 2 (/2012), 215–238.

Oberti, G., Bavestrello, F., Rossi, P.P., Flamigni, F., 1986. Rock mechanics investigations, design and construction of the Ridracoli dam. Rock Mech. Rock. Eng. 19, 113–142.
Pánek, T., Tábořík, P., Klimeš, J., Komárková, V., Hradecký, J., Šťastný, M., 2011. Deep-seated gravitational slope deformations in the highest parts of the Czech Flysch Carpathians: evolutionary model based on kinematic analysis, electrical imaging and trenching. Geomorphology 129, 92–112. https://doi.org/10.1016/j.geomorph.2011.01.016.
Pánek, T., Mentlík, P., Engel, Z., Braucher, R., Zondervan, A., 2017. Late Quaternary sackungen in the highest mountains of the Carpathians. Quat. Sci. Rev. 159, 47–62. https://doi.org/10.1016/j.quascirev.2017.01.008.
Pánek, T., Brezny, M., Kaapustava, V., Lenart, J., Chalupa, V., 2019. Large landslides and deep-seated gravitational slope deformations in the Czech Flysch Carpathians: new LiDAR-based inventory. Geomorphology 346, 106852. https://doi.org/10.1016/j.geomorph.2019.106852.
Pedrazzini, A., Jaboyedoff, M., Froese, C.R., Moreno, F., Langenberg, W., 2011. Structural analysis of Turtle Mountain: origin and influence of fractures in the development of rock slope failures. Geological Society London Special Publications 351 (1), 163–183. https://doi.org/10.1144/SP351.9.
Penna, I.M., Abellán, A., Humair, F., Jaboyedoff, M., Daicz, S., Fauqué, L., 2017. The role of tectonic deformation on rock avalanche occurrence in the Pampeanas Ranges, Argentina. Geomorphology 289, 18–26. https://doi.org/10.1016/j.geomorph.2016.07.006.
Radbruch-Hall, D., 1978. Gravitational creep of rock masses on slopes. In: Voight, B. (Ed.), Rockslides and Avalanches Natural Phenomena. Developments in Geotechnical Engineering. vol. 14. Elsevier, Amsterdam, pp. 608–657.
Riquelme, A.J., Abellán, A., Tomás, R., Jaboyedoff, M., 2014. A new approach for semi-automatic rock mass joints recognition from 3D point clouds. Comput. Geosci. 68, 38–52. https://doi.org/10.1016/j.cageo.2014.03.014.
Saintot, A., Henderson, I.H.C., Derron, M.H., 2011. Inheritance of ductile and brittle structures in the development of large rock slope instabilities: examples from western Norway. Geol. Soc. Lond., Spec. Publ. 351, 27–78. https://doi.org/10.1144/SP351.3.
Scarascia-Mugnozza, G., Bianchi-Fasani, G., Esposito, C., Martino, S., Saroli, M., Di Luzio E., Evans, S.G., 2006. Rock avalanche and mountain slope deformation in a convex, dip-slope: the case of the Majella Massif (central Italy). in: Evans, S.G., Scarascia Mugnozza, G., Ermanns, R., Strom, A., (Eds.), Massive rock slope failure. Nato Science Series Book, Kluiver Academic Publisher, the Netherlands, pp. 357–376.
Soldati M., 2013. Deep-seated Gravitational Slope Deformation, in: Bobrowsky, P.T., (Ed.), Encyclopedia of Natural Hazards. Encyclopedia of Earth Sciences Series. Springer, Dordrecht., pp. 151–155. doi:https://doi.org/10.1007/978-1-4020-4399-4_86.
Stead, D., Wolter, A., 2015. Critical review of rock slope failure mechanisms: the importance of structural geology. J. Struct. Geol. 74, 1–23. https://doi.org/10.1016/j.jsg.2015.02.002.
Suppe, J., Medwedeff, D., 1990. Geometry and kinematics of fault-propagation folding. Eclogae Geol. Helv. 83, 409–454.
Ter-Stepanian, G., 1966. Types of depth creep of slopes in rock masses. Proc. 1st Congr. Int. Soc. Rock Mechanics, Lisbon 2, 71–79.
Troiani, F., Della Seta, M., 2008. The use of the Stream Length-Gradient Index in morphotectonic analysis of small catchments: a case study from Central Italy. Geomorphology 102 (1), 159–168. https://doi.org/10.1016/j.geomorph.2007.06.02.
Troiani, F., Piacentini, D., Della Seta, M., Galve, J.P., 2017. Stream Length-gradient Hotspot and Cluster Analysis (SL-HCA) to fine-tune the detection and interpretation of knickzones on longitudinal profiles. Catena 156, 30–41. https://doi.org/10.1016/j.catena.2017.03.015.
Varnes, D.J., 1978. Slope movement types and processes, in: Schuster, R.L., Krizek, R.J., (Eds.), Landslides, analysis and control. Transportation Research Board Special Report 176, Nat. Acad. of Sciences, pp. 11–33.
Wegmann, K.W., Pazzaglia, F.J., 2009. Late Quaternary fluvial terraces of the Romagna and Marche Apennines, Italy: climatic, lithologic, and tectonic controls on terrace genesis in an active orogen. Quat. Sci. Rev. 28, 137–165. https://doi.org/10.1016/j.quascirev.2008.10.006.
Zischinsky, U., 1966. On the deformation of high slopes. Proc. 1st Congr. Int. Soc. Rock Mechanics, Lisbon 2, 179–185.